Strål säkerhets myndigheten
Swedish Radiation Safety Authority

Authors: Olle Lundh
Ylva Ranebo
Kristoffer Svendsen

Lunds universitet, Lund

Research

2019:04

Dosimetry in environments surrounding a laser-plasma accelerator

Report number: 2019:04 **ISSN:** 2000-0456
Available at www.stralsakerhetsmyndigheten.se

SSM perspective

Background

Modern laser technology makes it possible to generate ultrashort pulses with a very high peak power. At the Lund Laser Centre, a high-power laser facility in Lund, Sweden, laser pulses having a duration of approximately 30 femtoseconds are generated with a maximum peak power of up to 40 terawatts. When these pulses are focused, extreme light intensity is achieved. For example, when atoms in a gas are hit by these pulses, they are ionised almost instantaneously, resulting in the main part of the laser pulse interacting with a plasma consisting of free, negatively charged electrons and positively charged ions. The electrons are quickly displaced by the laser pulse whereas the heavier ions largely remain in place, resulting in a very strong electrical field.

The research conducted in the field is spurred by the potential to create applications where charged particles are accelerated to relativistic energies over very short distances in the strong electrical fields. This technology may allow for the development of new and much smaller types of accelerators for applications where for instance linear accelerators are used today.

Ionising radiation occurs around these laser plasma accelerators in connection with a range of different processes, both when the laser pulse interacts with the plasma, and when the accelerated particle beam is slowed down. It is well documented in the literature that ionising radiation is generated when this technology is used; however, the Swedish Radiation Safety Authority (SSM) has, from the perspective of radiation protection, identified the need for both an overall analysis and in-depth knowledge relating to the radiation environment around laser plasma accelerators.

Outcomes

This report demonstrates that the ionising radiation generated around laser plasma accelerators has a strong correlation to the peak power of the laser pulses. Nonetheless, the experimental arrangements can show great variation, for which reason general conclusions cannot be drawn.

Relevance

This report gives insight into the radiation environment around laser plasma accelerators from the perspective of radiation protection, and may be used as a tool for supporting SSM's licensing reviews and regulatory supervision in this field.

Need for further research

Depending on technological progress and its possible impact on the radiation environment around the equipment in question, a follow-up study may eventually be required, not only as a basis for updating SSM's framework of rules, but also to underpin licensing reviews and supervisory work in the field.

Project information
Contact person at SSM: Pia Eriksson
Reference: SSM2017-2478/7030171-00

Strål
säkerhets
myndigheten
Swedish Radiation Safety Authority

Authors: Olle Lundh
Ylva Ranebo
Kristoffer Svendsen

Lunds universitet, Lund

2019:04

Dosimetry in environments surrounding a laser-plasma accelerator

Date: January 2018
Report number: 2019:04 **ISSN:** 2000-0456
Available at www.stralsakerhetsmyndigheten.se

Dosimetry in environments surrounding a laser-plasma accelerator

Ylva Ranebo, Kristoffer Svendsen, Olle Lundh

Department of Physics, Lund University

Summary

Relativistic particle beams are unique tools for the exploration of the frontiers of physics: whether they are used in a particle collider to explore the subatomic world, or to generate X-rays that allow the structure and dynamics of atoms and molecules to be studied. The most powerful particle accelerators can be several kilometers in length and are thus very expensive to build and operate. A new promising method of particle acceleration based on high-power lasers has emerged, allowing significant reductions in both size and cost. When a high-power laser pulse is focused into a gas or a solid target, a plasma is created in which femtosecond or picosecond pulses of charged particles can be accelerated to hundreds of mega-electron-volts, or even more, in an acceleration distance of only a few millimeters.

This report considers laser-plasma acceleration from a radiation protection point of view. An overview is presented of the current status of research on ionizing radiation and radiation doses in the field of laser-plasma acceleration. The generation of ionizing radiation at laser-plasma accelerators is well-documented in the literature, as is the necessity of shielding to ensure personnel safety and to comply with regulations on radiation safety. Laser-plasma-accelerated beams have two specific features: i) the radiation is zero between the extremely short-duration pulses, and ii) the radiation hazards can be well isolated due to the very short acceleration length. However, the secondary radiation field will not differ greatly from that generated when a beam produced with conventional acceleration techniques interacts with matter. It is shown that the magnitude of radiation fields is strongly dependent on the power of the laser pulse and varies considerably between different laboratories. The experimental conditions and goals at each laboratory can also vary greatly, resulting in considerable variations in the number of particles accelerated, which makes general predictions difficult.

Various modeling and simulation methods for estimating radiation fields at laser-plasma accelerators are reviewed. The radiation fields generated during electron- and proton-acceleration experiments at the Lund multi-terawatt Laser Centre were investigated using the FLUKA transport code, in order to demonstrate the usefulness of Monte Carlo simulations. Regarding dosimetry and instrument response, it is also shown that many techniques used for monitoring continuous radiation can be applied to other accelerator fields operating in ultra-short pulsed mode, as long as certain precautions are taken.

Sammanfattning

Partiklar som accelereras till höga hastigheter är ett unikt redskap i en rad olika vetenskapliga områden. Till exempel inom materialforskning för utveckling av nya läkemedel eller bränsleceller till stora projekt inom högenergifysik som bl.a. bedrivs i CERN. Synkrotronljus som avges från accelererade elektroner kan användas för att undersöka ett materials egenskaper på atom- och molekylnivå eller för att studera kemiska reaktioner under mycket korta tidsförlopp. Avancerade experiment när partiklar accelereras och kolliderar görs för att undersöka naturens allra minsta beståndsdelar och universums historia. Men de kraftfullaste partikelacceleratorerna kan sträcka sig flera kilometer och är mycket kostsamma. I ljuset av detta har en ny teknik utvecklats, laserplasmaacceleration, baserad på högeffektlasrar som kan korta accelerationssträckan med flera tiopotenser. Genom att rikta en laserpuls på en gas eller ett fast mål, bildas ett plasma där laddade partiklar i femto- till pikosekunder långa pulser accelereras till hundratals megaelektronvolt eller mer, på bara några millimeters accelerationslängd.

Föreliggande rapport redovisar en studie på laserplasmaacceleration utifrån ett strålskyddsperspektiv med syfte att fördjupa kunskapen inom detta område. En översikt ges över det nuvarande forskningsläget om joniserande strålning och stråldoser i olika typer av laserplasmaanläggningar. Att joniserande strålning genereras då tekniken används är väl dokumenterat i litteraturen och att strålskärmning behövs för personalens säkerhet samt för att följa grundläggande säkerhetsnormer. Två specifika egenskaper för laserplasmaaccelererade strålar är att i) i stort sett ingen strålning existerar mellan de extremt korta pulserna, och ii) strålningsfaran kan bli väl isolerad på grund av den väldigt korta accelerationssträckan som tekniken använder sig av. Däremot kommer strålningen som skapas inte att vara annorlunda från vad som uppkommer då en liknande stråle som genererats vid en konventionell accelerator växelverkar med omgivande material. Rapporten visar att strålningen som genereras är starkt beroende på vilken pulseffekt lasersystemet kan leverera. Dock kan de experimentella uppställningarna vid varje laboratorium variera stort och därmed medges inte allmängiltiga slutsatser.

En genomgång ges av olika modellerings- och simuleringsmetoder lämpade för uppskattning av strålmiljöer vid laserplasmaacceleratorer. Monte Carlo-programmet FLUKA har använts i syfte att demonstrera ett sådant simuleringsverktyg och att karakterisera strålmiljön som alstras vid elektron- respektive protonacceleration vid multi-terawatt lasern vid Lunds Lasercentrum. För att utreda instrumentrespons och dosimetriska mätningar vid laserplasmaacceleratorer, kan kunskap tillämpas från andra fält där acceleratorer också används i ultrakorta, högintensiva pulser, t.ex. synkrotronljusanläggningar och linjäracceleratorer. Tekniker som används för kontinuerliga strålfält kan också användas i pulsade, högintensiva fält så länge beaktande tas vid val av instrument, såsom om primär- eller sekundärstrålning ska mätas.

Abbreviations and notations

CPA	chirped pulse amplification
EPD	electronic personal dosimeter
ICRP	International Commission for Radiation Protection
ICRU	International Commission on Radiation Units and Measurements
LLC	Lund Laser Centre
LWFA	Laser Wakefield Acceleration
NCRP	National Council on Radiation Protection and Measurements
OSL	optically stimulated luminescence
PIC	particle-in-cell
Ti:sapphire	titanium-doped sapphire
TNSA	target-normal sheath acceleration
TLD	thermoluminescence dosimeter

E	energy
e^-	electron
k_B	the Boltzmann constant
n	neutron
p	proton
T_{hot}	hot electron temperature
Z	atomic number

Contents

1 Introduction

1.1 Background

Modern science and technology employ beams from particle accelerators as an essential tool in a wide range of applications. Higher energies and higher particle beam quality are required to answer some of the most fundamental questions regarding the origin of our universe, the nature of dark matter, space and time, and the elementary constituents of matter. However, higher energy usually means a higher cost.

Today's conventional accelerators use electric fields generated by radio waves to accelerate electrons and other charged particles to velocities approaching the speed of light. However, the particle energy attainable is constrained by the electric field strength. Breakdown, arcing and even melting of the metallic accelerating structures, will result at a field above a few tens of megavolts per meter. Thus, it is necessary to build longer, more complex and costlier accelerators in order to achieve higher particle energies.

In research on laser-plasma acceleration, new techniques are being studied to accelerate particles by taking advantage of the strong electromagnetic fields that can be sustained in a plasma. In 1979, Tajima and Dawson from the University of California presented and proved a theory that elementary particles could "surf a plasma wave" and be accelerated to relativistic velocities in a few centimeters (Tajima and Dawson, 1979). The electromagnetic energy from a laser pulse is transformed into the kinetic energy of particles, and the first experiments confirming this were performed during the 1980s (Clayton et al., 1985). Later experiments have shown acceleration in electric fields of tens, even hundreds of gigavolts per meter, leading to more than 1000 times higher particle energies per unit length of acceleration than in conventional accelerators. Plasma accelerators could therefore constitute short, yet very powerful, accelerators.

Laser-plasma acceleration has led to a new branch of radiation protection as laser-matter interactions can generate highly energetic accelerated particles. Electron beams with energies in the range of GeV and proton beams of several tens of MeV both constitute a radiological risk.

1.2 Objectives

This report presents a study on radiation protection aspects in the operation of different kinds of laser-plasma accelerator facilities. The aims of this report are:

- to give an overview of the current status of research on ionizing radiation and radiation doses in the field of laser-plasma acceleration,
- to provide an analysis of the types of radiation and radiation doses that workers can be expected to be exposed to,
- to provide suggestions for appropriate instruments for measuring radiation doses in environments where charged particles are accelerated in very short pulses with high intensity,
- to review the possibilities, difficulties, and applicability of existing simulation programs for these radiation environments, and
- to give an overview of technology development and the expected increase in use of laser-plasma acceleration.

2 Laser-plasma acceleration

In order to understand one of the key concepts behind laser-plasma acceleration, we will first consider some basic physics. Power is defined as the amount of energy supplied, or expended, during a period of time. Let us assume that we have a laser pulse with an energy of 1 joule, which is about the energy required to lift an apple one meter. If this laser pulse is compressed to an infinitesimally short period of time, such as 50 femtoseconds (50/1,000,000,000,000,000 of a second), then the power will be: 1 J / 50 fs = 20 TW. This quantity is so great that it exceeds five times the whole world's nuclear power capacity of 400 GW (World Nuclear Association, 2017).

To achieve powers up to petawatts (10^{15} W) in laser-plasma acceleration, a laser pulse of a reasonable energy, say 1–100 J, but with an infinitesimally short duration of femto- to picoseconds, is aimed at a target. When this power is focused into a spot about a micrometer in diameter, intensities of 10^{20} W cm^{-2} can be achieved. Such an intensity will lead to the formation of a plasma of the target material that is able to sustain electric fields so high that they can accelerate charged particles to relativistic energies.

However, such high laser intensities would destroy the optical components and damage the beam optics in the system. In the 1980s, a new technique called chirped[1] pulse amplification (CPA) revolutionized laser technology, increasing the highest power that could be delivered immensely (Strickland and Mourou, 1985). The technique makes use of the fact that the peak power of a pulse can be reduced by stretching the pulse in time. Very short pulses contain many wavelengths that can be spatially dispersed by an arrangement of gratings so that shorter wavelengths travel a longer optical path length. Longer wavelengths will thus exit the stretcher before the shorter wavelengths, resulting in a longer (stretched) pulse. In this way, the peak power of the pulse can be reduced, allowing massive amplification before the pulse is recompressed and focused onto the target.

In the following sections, a short description is given of the mechanisms behind the generation of electron and proton beams. For a more detailed description of the processes, the reader is referred to publications by Esarey et al. (2009), Corde et al. (2013) and Daido et al. (2012).

2.1 Generation of electron beams

When an ultra-intense laser pulse hits a gas jet, a plasma is formed after electrons are stripped off the atoms by the pulse front. A plasma is the fourth state of matter (the others being solid, liquid and gas), and can be pictured as an electrically neutral gas composed of free-floating electrons and positively charged ions. The pulse then propagates through the plasma like a bullet, and electrons are deflected from their paths on the time-scale of the pulse duration, while the motion of the much heavier positive ions is almost unaffected. The electrons start to oscillate around their initial position as they are drawn back by the positive ions, passing back and forth over the direction of propagation of the laser pulse. The laser pulse has thus excited a longitudinal charge wave of oscillating electrons.

[1] The wavelength of the laser pulse is increased or decreased linearly with time, in the same way as the sound when a bird is chirping.

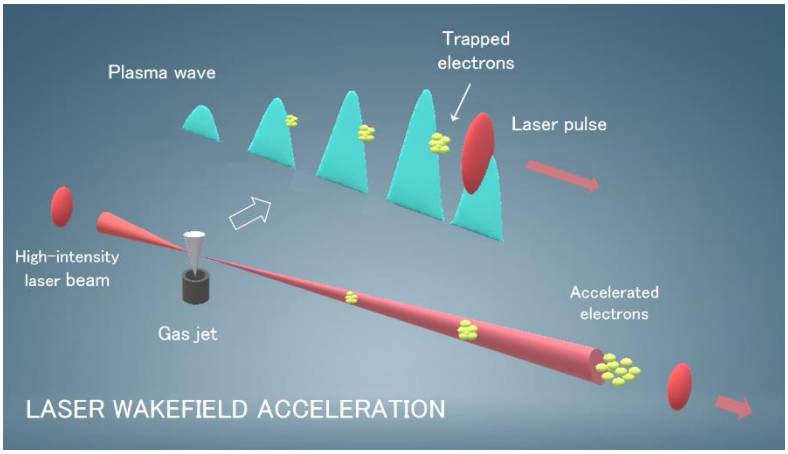

Figure 2.1: Schematic of laser wakefield acceleration. The pulse excites a plasma wave leading to trapping of electrons in the wake. These will be sequentially accelerated in the strong electrical field that results from the slow positive ions and the plasma electrons.

Immediately after the pulse there is an electron-free "bubble" containing only slow positive ions. This bubble is surrounded by a region with a high density of electrons that forms a "wake" behind the bubble. If electrons are injected into this wake at exactly the right moment, they can be accelerated in the same manner as a surfer riding an ocean wave. Sequential acceleration will take place in the strong electric field in the bubble resulting from the heavy positive ions and the surrounding electrons. This process, called laser wakefield acceleration (LWFA), is illustrated in Figs. 2.1 and 2.2.

In the plasma wave, the amplitude of the (for electrons) accelerating electric field strength can reach hundreds of gigavolt per meter, which is a thousand times higher than that used in conventional particle accelerators. At such field strengths, electrons can be accelerated to record-breaking energies of GeV over distances of a few centimeters, and hundreds of MeV in less than a millimeter. However, the short acceleration distance is also one of the problematic characteristics of the technique, as it is crucial that the electrons are injected at exactly the right moment in time, which is difficult as it requires micrometer precision. Electron injection is thus an important subject of research in the field.

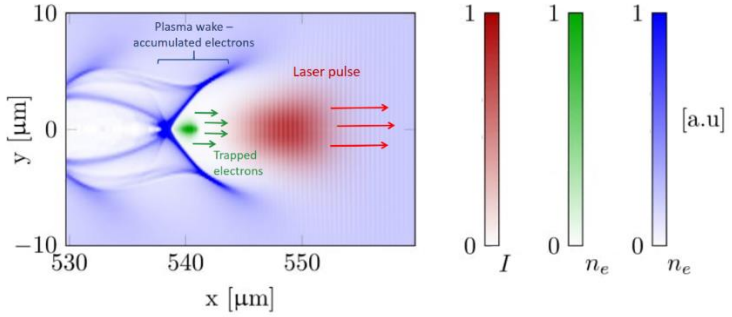

Figure 2.2: Illustration of the wake and the electron acceleration mechanism. The plasma electron density (n_e), illustrated in blue, shows the accumulation of electrons forming a wake behind the laser pulse, shown in red (with intensity, I). In this case, the pulse has travelled 55 µm into the gas jet and formed a bubble with a diameter of ~10 µm. The white areas are electron-free regions and the green area indicates the electrons trapped in the wake. (Graphics from a simulation by H. Ekerfelt and M. Hansson, Atomic Physics, Lund University.)

2.2 Generation of proton and ion beams

The acceleration of protons and ions relies on a different mechanism than electron acceleration. It is today not possible to accelerate ions with a plasma wave, as the injected particles would have to travel close to the speed of light, which for protons would mean energies in the GeV range. At lower particle velocities, the wave oscillations would be too fast, resulting in a net average acceleration of zero. Instead, an electric field that changes so slowly that it is almost static in relation to the motion of the ions is used in plasma ion acceleration.

Proton beams in the ten MeV range resulting from laser–solid interactions were observed for the first time in 2000 (e.g., Clark et al., 2000). However, the theory describing the acceleration mechanisms is complex, and is still not completely understood. Several theories were proposed during the following years. One of the issues debated was from which side of the target the ions were accelerated (Macchi et al., 2013). In the target-normal sheath acceleration (TNSA) model proposed by Wilks et al. (2001), the ions are assumed to be accelerated from the rear of the target, i.e., the opposite side to the laser-irradiated surface, based on experimental evidence. Today, the results from most experiments are interpreted using the TNSA model, which is illustrated in Fig. 2.3. Other acceleration mechanisms have also been proposed, see, for example, the review by Borghesi et al. (2006). Fig. 2.4 shows a photograph of laser-driven ion acceleration from a thin metallic foil target taken during experiments reported by Lundh (2008). The target is usually a metallic foil, a few micrometers in thickness.

The TNSA model can be simply described as plasma expansion resulting from a high-intensity laser pulse (>10^{18} W cm^{-2}) hitting a target. A fraction of the energy of the laser pulse will be transferred to the electrons in the target material, forming so-called hot electrons. These will be forced into the target and, at a point determined by the electron density, the pulse will be reflected. Hot electrons can be accelerated to relativistic energies, and they propagate through the target and may finally escape. Charge separation arises in the vacuum between the escaping electrons and the remaining positive regions. The electric field generated in this way appears to be static relative to the motion of the slow ions as its duration is on the order of picoseconds. This field is strong enough to ionize hydrocarbon and water atoms on the rear of the target, which can then be accelerated up to the MeV range.

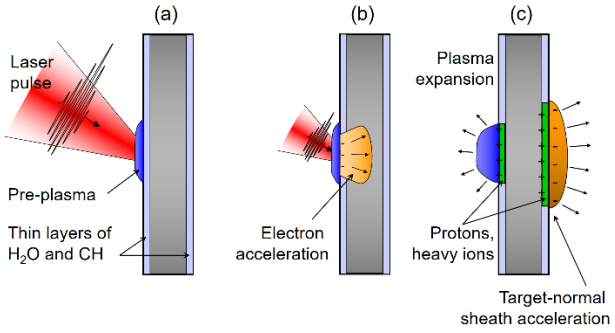

Figure 2.3: Illustration of ion acceleration in the TNSA regime. a) An intense laser pulse creates an expanding plasma of hot electrons at the front of the target. b) The laser pulse drives hot electrons into the target. c) An electron sheath is formed at the rear of the target, and charge separation sets up a strong quasi-static electric field in vacuum. The strong field (on the order of TV m^{-1}) ionizes surface atoms, and the positive ions can be accelerated up to tens of MeV.

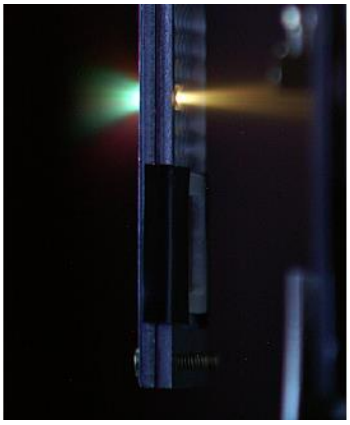

Figure. 2.4: Photograph of proton acceleration from a thin foil target taken during a laser-plasma acceleration experiment. A high-intensity laser pulse, incident from the left, hits the front of 6 µm copper foil, accelerating ions from the back of the foil along its normal direction, towards the right.

2.3 Radiological protection and sources of ionizing radiation

Experiments involving laser-matter interactions at ultra-high laser intensities often result in the emission of energetic particles, for example electrons, protons and ions. In particular, a laser-plasma accelerator can produce beams of particles with preferential direction and small divergence angle. The energy distribution and type of these primary particles strongly depend on the laser parameters and on other experimental conditions. The primary particle beam is emitted with a certain divergence but is often also dispersed by magnetic fields in the experimental instrumentation. Secondary particles are produced when the particle beam encounters materials surrounding the experiment, e.g. the interaction chamber and the concrete walls of the experimental hall. The secondary particle types depend on the type of primary particle, its energy, and on the materials in the beam path. The secondary radiation which contributes to the radiation environment consists mostly of low energy electrons from electronic collisions, gamma rays, bremsstrahlung and neutrons from nuclear reactions, e.g. (γ,*n*) and (p,*n*) reactions. Other, more exotic particles such as positrons and muons can be generated but for the energies obtained from laser-plasma accelerators, their contribution to the radiation environment is normally small. Nuclear reactions can also lead to activation and production of radioactive isotopes. However, analysis shows that, in most cases activated isotopes are relatively few and short-lived (see Section 4.2).

The primary radiation is produced in very short pulses at the source (femtoseconds), but spreads temporally during propagation due to divergence, energy spread, and dispersion in magnetic fields. Furthermore, secondary radiation is produced in several geometrical locations surrounding the experiment. This geometrical effect results in effectively longer exposure (nanosecond).

First estimates of the radiation environment can be done using analytic models and estimates of conversion factors and attenuation coefficients in radioprotective barriers. For more exact assessments, Monte-Carlo simulations are required. In the design of radioprotection, the directionality of the primary and secondary radiation should be considered, so that the exposure is kept as low as possible. Here, the

compactness of laser-plasma accelerators is an advantage, since the radiation hazards can be isolated inside the interaction chamber, and the useful beam extracted through dedicated openings.

The estimates of risk and exposure in the environment surrounding a laser-plasma accelerator, include the instantaneous dose (produced in a single laser shot) and average dose (the dose obtained over an extended period, e.g. from all laser shots during one year). Some lasers are very powerful, but deliver only a few shots per day, while other lasers are less powerful, but deliver many shots per second. Therefore, both the laser power and the repetition rate are important factors when assessing the yearly dose.

Conversion coefficients are used in radiological protection to calculate different quantities for different particle types and energies. Figure 2.5 shows the conversion of particle flux (particles per unit area) to effective dose coefficients for electrons, photons and neutrons as a function of energy in an anterior-posterior (front to back) irradiation geometry. It can be seen from this diagram that, even for a low particle energy, the resulting effective dose can be significant if the flux is high.

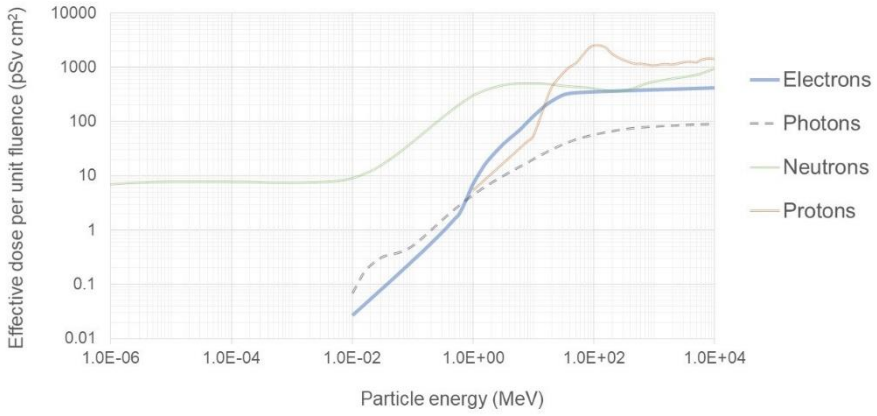

Figure 2.5: Conversion coefficients from particle flux to effective dose for anterior-posterior irradiation (ICRP, 2010).

In laser–solid interactions, the energetic electrons generated will lead to secondary radiation, mainly X-rays, γ-rays and electrons, with a maximum energy equal to that of the incident electron. The energy spectrum of these hot electrons can be described by a Maxwellian probability distribution:

$$\frac{dN}{dE} \propto \sqrt{E} \cdot e^{-\frac{E}{k_B T}} = \sqrt{E} \cdot e^{-\frac{E}{T_{hot}}}$$

where N denotes the number of electrons, E is the electron energy, k_B is the Boltzmann constant and T is the temperature of the plasma. In plasma physics literature, T_{hot} is often denoted as a temperature, but it is actually a measure of electron energy. This notation is derived from the fact that the temperature of a system is always related to the energy distribution of its constituents, i.e., the probability that a particle has a specific energy. T_{hot} [eV] is the product of the temperature [K] and the Boltzmann constant [eV K^{-1}].

The electron energy derived from scaling laws by Wilks and William (1997), Beg et al. (1997) and Haines et al. (2009) is plotted versus laser intensity in Fig. 2.6, for the specific wavelength of 800 nm. Considering that the range of an electron in water is about 0.001–1 mm for an electron temperature of 10–100 keV, this could be used as a limit at which the electrons can penetrate the skin.

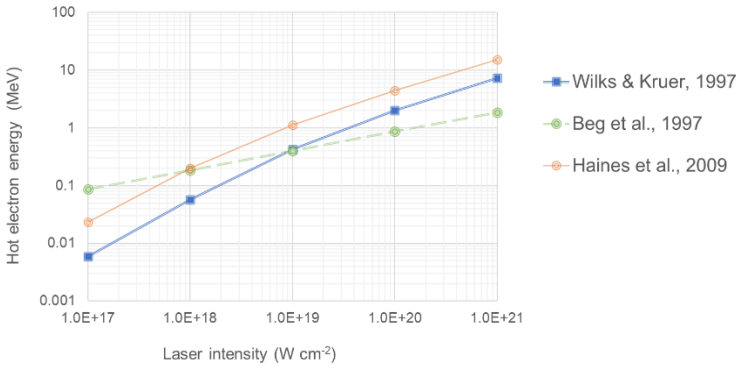

Figure 2.6. Hot electron energy (temperature) versus laser intensity on the target for a wavelength of 800 nm. (Adapted from the work of Wilks and William (1997), Beg et al. (1997) and Haines et al. (2009).)

According to Fig. 2.6, this gives a rough estimate of the threshold at which laser–solid interactions produce ionizing radiation and ionization in body tissue, of about 10^{17} W cm^{-2} for a laser wavelength of 800 nm. It should be emphasized that this is only a rough estimate, as other factors must also be taken into account, such as the density and elemental composition of the target.

2.4 A laser-plasma acceleration laboratory

The high-power laser facility at the Lund Laser Centre (LLC), Sweden, houses a titanium-doped sapphire (Ti:sapphire) laser system utilizing the technique of CPA to obtain short, high-contrast laser pulses with energies of more than 1 J on target. The peak power of each laser pulse can reach 40 TW, with a pulse duration of 30 fs. When focused, it is possible to achieve intensities greater than 10^{19} Wcm^{-2}. To accelerate electrons, the laser is typically focused in a gas cell, or in a gas jet, approximately once every 10 seconds. Protons are accelerated by focusing the laser onto a thin metallic foil, such as aluminum, copper or gold, that is repositioned after each laser shot. In these experiments, electrons can reach energies of 300 MeV, whereas protons can reach up to 10 MeV.

Layout of the facility

A schematic illustration of the LLC multi-terawatt laser system is given in Fig. 2.7. The system relies on the generation and amplification of very short pulses in the femtosecond domain. The duration depends on the frequency bandwidth of the laser medium. This is the reason why Ti:sapphire, with a broad gain profile centered around 800 nm, is used. In the CPA laser chain, labelled *Stretcher* in Fig. 2.7, the short oscillator pulses are stretched from the femtosecond to the picosecond domain, before being amplified. neodymium-doped YAG lasers are used to pump the amplification stages. A reciprocal arrangement of gratings recompresses the pulses to 30 fs and 40 TW peak power at the end of the laser chain. At such peak power, the compressed

pulse cannot propagate through air, and is transported in vacuum to the experimental stations.

The facility is located in the basement of the Department of Physics at Lund University. Interior views are shown in Fig. 2.8. The laser beam can be sent to two experimental stations in an adjoining room (Fig. 2.9), but only one station can be used at a time. Experiments involving solid targets, i.e., proton acceleration, are performed in the outer laboratory, the High-Intensity Room. Electron acceleration is performed in the inner room, called the Electron Acceleration Room, which was constructed underground, outside the main building, in 2012.

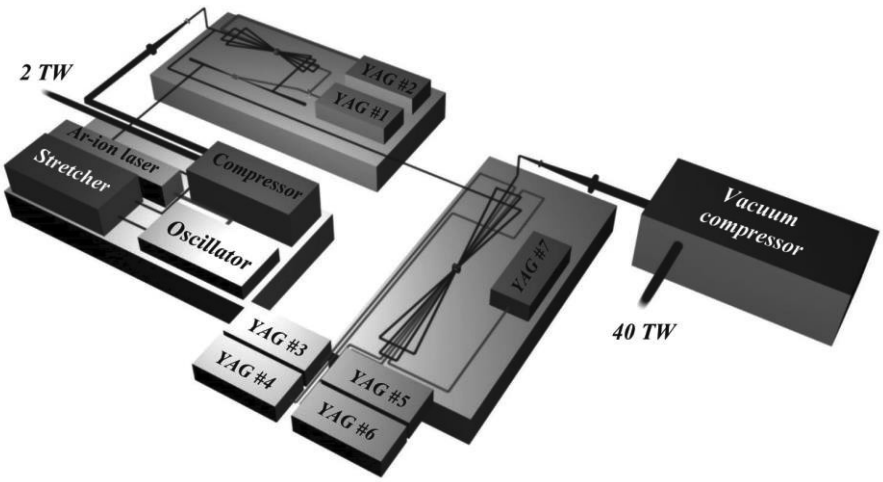

Figure 2.7: Schematic view of the Lund multi-terawatt laser system.

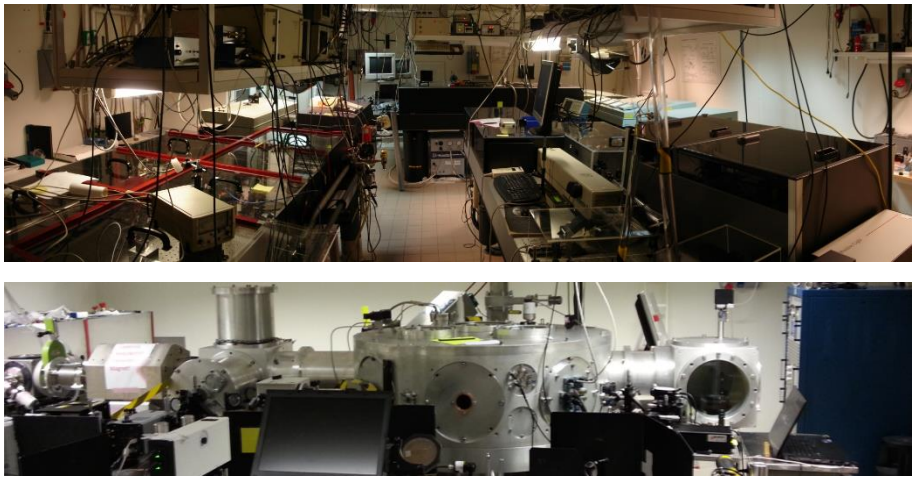

Figure 2.8: The upper picture shows a view of the Multi-Terawatt Laser Room with the oscillator, stretcher and compressor inside the boxes on the right. The lower picture shows a view of the aluminum experimental chamber for electron acceleration. The laser pulse enters from the right and the electron beam is generated at the center of the cylindrical chamber. The beam then propagates towards the far end of the room, to the left in the picture.

The inner and outer laboratories are separated by a 60-cm thick concrete wall, and the opening between the rooms is covered with a 13-cm thick sliding lead door. Each cylindrical experimental vacuum chamber is made of aluminum, is 120 cm in diameter, 60 cm high, and has 5 cm thick walls. The electron beam is generated in the center of the chamber, and propagates away from the door, towards the far end of the room. Radiation in the forward beam direction is absorbed in the far concrete wall, or in the soil outside the Electron Acceleration Room. In the High-Intensity Room, the protons are generated in the center of the chamber but stopped by the chamber walls. One control desk is used for all experiments and is placed behind a lead wall in the High-Intensity Room.

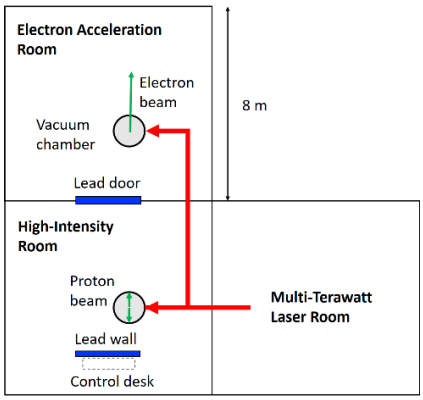

Figure 2.9: Layout of the experimental area at LLC. The laser room and the control room are in the basement of the main building, while the Electron Acceleration Room is outside the main building in an underground bunker, which is sealed by a lead door. The electron beam propagates away from the main building.

Repetition rate and annual shot rate

Although the laser operates at 10 Hz, electron beams are produced at a maximum rate of 0.1 Hz. The reason for this is that gas used as the target to provide the plasma for the previous shot must be pumped out of the vacuum chamber prior to the next shot, which takes about 10 seconds. Before each experiment, the laser and auxiliary equipment must be prepared, which takes a few hours. When modifications are made to the setup, the vacuum chamber must be opened and then evacuated, which takes at least an hour. Therefore, in a typical day, 100–1000, but never more than 3000, laser shots are used in an electron acceleration experiment. Taking into account the time required for laser maintenance, and that the laser is also used for other experiments, it is estimated that electron beams are generated during less than 100 days per year, giving a maximum of 100,000 laser shots. To date, however, no more than 50,000 shots have been fired in any single year. Assuming an average charge of 100 pC per shot, this gives an estimated maximum total charge of 10 μC ($6.2 \cdot 10^{13}$ electrons) per year.

Proton beams can be produced at a maximum rate of 0.01 Hz (less than 1 shot/minute). The reason for this is that on each shot, the target foil is destroyed and a new foil has to be accurately positioned, with micrometer precision, prior to the next shot. This process typically requires at least one minute, often more. Moreover, the target foil holder typically contains less than 100 individual targets and to change it, the vacuum chamber must be opened. Therefore, in a typical day, less than 100, and never more than 300 laser shots are used for proton acceleration experiments. Assuming 5,000 shots per year, gives an estimated maximum number of 10^{14} protons per year, with energies in the range of 1-10 MeV.

Since the electron beam is more energetic, and is generated at a higher repetition rate than the proton beam, electron acceleration experiments are expected to generate significantly more radiation annually than the proton acceleration experiments.

A laser-plasma acceleration experiment

As mentioned above, it is crucial to inject the electrons into the plasma wave at exactly the right moment. There are several ways in which this can be achieved experimentally. In the bubble regime, the plasma wave becomes severely nonlinear, and transverse wave breaking effects can result in self-injection of electrons. Unfortunately, self-injection is difficult to control, and it is not applicable when fine-tuning and control of the injected electron bunch are required.

An important part of the research program at the LLC is the development and improvement of different injection techniques. The aim in many experiments is to produce electron beams with high quality, i.e. with a narrow energy spread. This can be done by localizing the injection in space so that all the electrons are accelerated over the same distance and gain the same energy. Colliding pulse injection is one example of an injection technique. Here electrons are injected locally following the collision between the main pump pulse and a weaker, counter-propagating injection laser pulse (see Figs. 2.10 and 2.11).

It is also possible to modulate the plasma density profile and inject electrons in a density down-ramp, or in a shock-front in a supersonic gas flow. Another possibility is to use mixtures of gases with different ionization potentials. Each injection mechanism leads to electron beams with different characteristics. The results obtained at the LLC are summarized in Table 2.1.

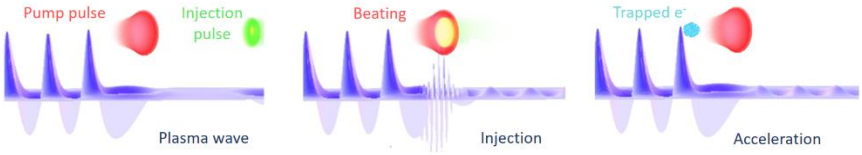

Figure 2.10: The principle of colliding pulse injection. An intense laser pulse (the pump pulse) drives a nonlinear plasma wave. In the injection phase, a weaker, counter-propagating laser pulse collides with the pump pulse and pre-accelerates background electrons. Pre-accelerated electrons are then trapped at the wake and accelerated by the plasma wave.

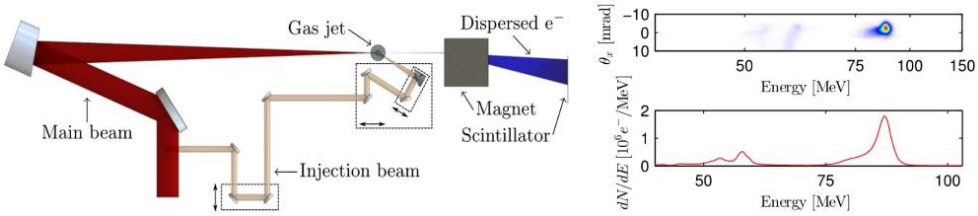

Figure 2.11: Setup and typical results from a colliding pulse injection experiment. A small fraction of the main laser pulse is split off and used as an injection pulse. The two pulses collide in a supersonic gas jet at an angle of 150°. A series of linear translation stages is used for accurate adjustment of the optical path difference and spatial overlap of the two pulses. The electron beam is analyzed using a dipole magnet and a scintillator screen. The top right panel shows a raw image of the screen, while the bottom panel shows the analyzed electron spectrum. Here, the peak energy is 86 MeV and the energy spread is 3 MeV (3.5%), which is the limit of the spectrometer resolution.

Table 2.1: Parameter range for the electron beams obtained using different injection mechanisms. The typical charge range is given per bunch (1 pC = $6.2 \cdot 10^6$ electrons). The energy range is the average energy. The energy spread (ΔE/E) and divergence were determined at full-width at half-maximum. The parameters are taken from recently published articles authored by researchers working at the LLC.

Injection mechanism	Charge [pC]	Energy range [MeV]	ΔE/E [%]	Divergence [mrad]	Publication
Self-injection	10–100	50–200	10–100	5–10	Mangles et al., 2006; Hansson et al., 2014; Svensson et al., 2016
Ionization	5–50	50–200	100	10	Hansson et al., 2016a; Desforges et al., 2016
Down-ramp	1–10	40–100	50	10	Hansson et al., 2015
Shock-front	1–10	40–100	5	5	Burza et al., 2013
Shock + ionization	1–10	80–150	7	4	Thaury et al., 2015
Colliding pulses	1–10	40–100	3	3	Hansson et al., 2016b

3 Survey of published radiological assessments for high-power laser facilities

This chapter presents a summary of a selection of published studies on radiation fields and radiation protection measures for different laser-plasma systems. The studies were categorized according to the peak power delivered by the system: GW (10^9 W), TW (10^{12} W) or PW (10^{15} W) lasers. The results for both laser–solid and laser–gas interactions are given for each power class, except for GW lasers, for which reports were found for one facility, both dealing with laser–solid experiments. A study on the radiation environment at the LLC is presented separately in Chapter 4.

Figure 3.1 shows the distribution of ultra-high intensity laser facilities around the world. The studies summarized originate from the following facilities.

- The 1 GW laser system at the Pulsed Laser Center (CLPU), Faculty of Physics, University of Salamanca, Spain.
- The 25 TW laser system at the Prague Asterix Laser System (PALS) Research Centre, Prague, Czech Republic.
- The 100 TW laser system at the Laboratory for the Use of Intense Lasers (LULI), École Polytechnique, Paris-Saclay University, France.
- The 2 × 10 PW laser system, under construction at the Extreme Light Infrastructure-Nuclear Physics (ELI-NP) Research Centre, Romania.

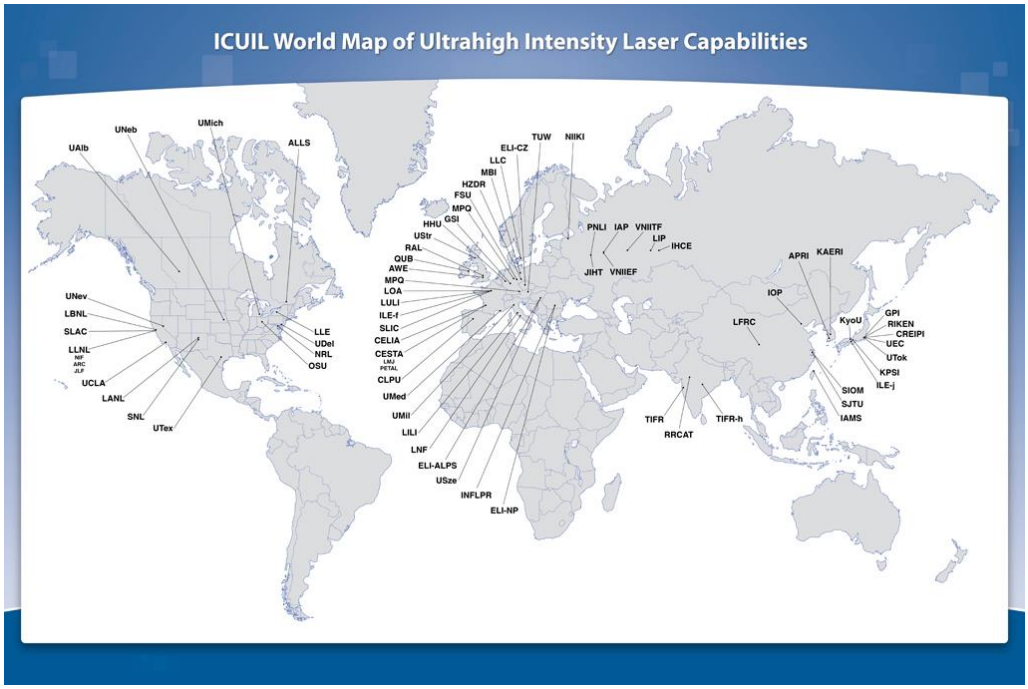

Figure 3.1: Map showing the distribution of ultra-high intensity laser facilities around the world. (Reproduced from the International Committee on Ultrahigh Intensity Lasers (ICUIL) World Map by Dr. C.P.J. Barty, from https://www.icuil.org/activities/laser-labs.html, retrieved October 24, 2017. Copyright 2015 ICUIL. Reprinted with permission.)

It should be emphasized that studies on radiation protection and shielding practices at high-intensity laser facilities are rather inhomogeneous and are only applicable for the specific conditions at each facility. However, these studies reveal that the generation of ionizing radiation is strongly dependent on the laser beam intensity and the type of laser–target interaction. Therefore, we have categorized the studies based on these parameters, as we believe this should give an adequate picture of the radiological environment at different types of facilities.

3.1 Gigawatt laser systems

Laser–solid interactions

Two studies have been published on laser–solid interactions at CLPU: *High Electron Doses from a GW Laser Interacting with Solid Aluminum Targets* (Fonseca et al., 2010a) and *Measurement of radiation produced by ultra-short laser pulses interacting with solid targets* (Fonseca et al., 2010b). The authors report γ and electron radiation measurements for a laser system with a power of 1 GW, interacting with a solid aluminum target. This system is a Ti:sapphire laser with a CPA amplifier that delivers pulses of 110 fs duration and an energy of 0.9 mJ at a repetition rate of 1 kHz. The intensity at the focus on the target was estimated to ~10^{16} W cm^{-2}.

About 900,000 shots were fired during a period of 15 minutes. Thermoluminescence dosimeters (TLDs) and radiochromic films were used to measure the dose as a function of distance. The particle energies were determined based on these data and stopping powers in air. The authors concluded that the emitted radiation consisted mainly of electrons described by two Maxwell–Boltzmann distributions with energies of some tens of keV. In addition, a smaller, but not insignificant, component of photons produced by bremsstrahlung emission was measured.

The authors reported a maximum dose rate of 8.25 μSv/s, with no discrimination between doses from electrons or photons, at a zero-degree reflection angle and a distance of 30 cm from the target. The dose rate decreased to 0.25 μSv/s at an angle of 180°. The authors concluded that, even for a low-power laser system, the high repetition rate led to a significant amount of radiation, which should be considered when designing such systems. However, radiation with an energy of tens of keV can be easily shielded against, and thin shielding with a material of low atomic number would be sufficient to eliminate any hazards from both β and bremsstrahlung.

3.2 Terawatt laser systems

Laser–gas interactions

Olsovcova et al. (2014c) evaluated the radiological hazards from a high-repetition-rate, high-intensity laser at the PALS Research Centre in Prague in a study entitled: *Radiation Protection Aspects in the Vicinity of TW Class Laser Systems*. The system is a 25 TW Ti:sapphire laser that provides a peak power of 25 TW in pulses <40 fs, with an energy of about 1 J. Typical experiments at the facility based on electron acceleration from a gaseous target were studied, both theoretically and experimentally, in order to verify the adequacy of existing bulk shielding and radiological safety. The responses of personal dosimeters in pulsed radiation fields, for which these dosimeters are not designed, were also evaluated.

The Monte Carlo transport code FLUKA (for a description, see Chapter 4) was used to simulate the electron, photon and neutron fluences, and ambient dose equivalents. The electron beam was attributed a mean energy of 100 MeV, a divergence of 10° and $6 \cdot 10^6$ electrons per shot. The interaction chambers were modeled as spherical steel shells with an outer diameter of 80 cm and a 1 cm thick wall. A sketch of the experimental arrangement is shown in Fig. 3.2. An activation study was also performed, in which a steel slab 1 cm thick was assumed to have been irradiated for 100 s by a 100 MeV electron beam. The induced radioactivity was calculated up to an hour after the end of irradiation.

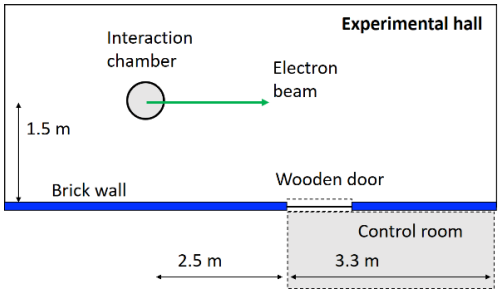

Figure 3.2: Schematic view of the experimental arrangement at the PALS high-intensity laser system. The interaction chamber was modeled as a steel chamber of diameter 80 cm and a 1 cm thick wall. A 15 cm thick brick wall with a 3 cm thick wooden door separated the control room from the experimental area.

Measurements were also performed with electronic personal dosimeters (Mk2 EPD 2.3, Thermo Scientific), TLDs and films (Foma Personal Monitoring Films). The dosimeters were positioned inside and outside the interaction chamber, in the experimental area and the laser control room, and exposed to radiation from 180 shots.

The fluences simulated with FLUKA showed that most of the particles and photons were emitted in the forward beam direction; the highest value being close to laser–gas interaction point, as expected. The wall of the interaction chamber was predicted to offer effective shielding, and decreased the fluences by several orders of magnitude. Neutrons were produced, but their fluence was many orders of magnitude lower than those of electrons and photons. Simulated and measured doses for 180 shots at different positions in the experimental area are given in Table 3.1.

Table 3.1: Dose equivalents for 180 shots obtained from FLUKA simulations and TLD and film measurements. The ranges of doses reflect the variation between different measurement positions.

Location	FLUKA [mSv]	TLD [mSv]	Film [mSv]		
			Photons	Electrons	Total
Interaction chamber (IC)	2.3–42	0.8–34	0.1–18	9.1–16	9–33
Vicinity of IC	0.2	Not measured	1.7	0.00	1.7
Experimental hall	≤ 0.1	≤ 0.3	≤ 0.5	0.00	≤ 0.5
Laser control room	0.00	Not measured	0.00	0.00	0.00

The simulations and responses of TLDs and films generally agreed well. Inside the interaction chamber the dose from γ-radiation constituted 1% to 50% of the total. The EPDs responded well and showed good agreement with the TLDs and FLUKA simulations, despite low expectations due to the short pulses and findings reported in another study (Borne et al., 2002). A possible explanation for the good agreement was suggested to be the distance to the EPDs, which the authors argued could be sufficient to prolong the pulse time.

The activity induced in the steel slab was low and consisted mainly of iron and vanadium isotopes (see Table 3.2). Activation products of air, ^{15}O and ^{13}N, were below 10^{-8} Bq cm^{-3}.

Table 3.2: FLUKA simulations of the activity induced in a 1 cm thick steel slab, after 100 seconds of irradiation with a 100 MeV electron beam. Only the most dominant nuclides are specified.

Nuclide	**Half-life [min]**	**Induced activity [mBq cm^{-3}]** Time after irradiation		
		10 sec	10 min	60 min
^{53m}Fe	2.58	5.0	0.4	0.00
^{53}Fe	8.51	2.3	1.8	0.03
^{52}V	3.743	0.4	0.1	0.00
Others		1.1	0.5	0.17

The authors concluded that typical experiments at the laboratory would not pose any radiation risk to personnel or the public as long as access to the experimental hall is prohibited during operation. The authors also simulated a maximal operational scenario of 240 shots per day, for which the more exposed parts of the laser control room showed an annual dose of 0.5 mSv. It was therefore recommended that occupancy of this room be kept to a minimum. Their results indicated that the EPD response was promising and that these could provide a supplement to passive dosimeters, but it was suggested that further studies should be carried out on their performance in pulsed fields.

Laser–solid interactions

The study by Borne et al. in 2002, *Radiation Protection for an Ultra-High Intensity Laser*, is one of the earliest published studies on radiation protection at high-intensity laser facilities, and is cited by many others. Borne et al. presented a thorough radiological study of the vicinity of a 100 TW Ti:sapphire/Nd:glass laser facility at LULI in Paris. Different techniques were used to measure γ- and neutron radiation for different laser pulse energies and intensities on solid and semi-solid targets. Levels of activation and contamination were also investigated.

The LULI 100 TW laser system is based on the CPA technique applied to Nd:glass and Ti:sapphire amplifiers. The maximum energy the system can deliver is 30 J and 15 J with pulse durations of 300 fs and 350 fs, respectively. The maximum repetition rate is one shot every 20 minutes. The spherical experimental chamber is composed of stainless steel, and is 1 m in diameter with a mean wall thickness of 1 cm. It has several windows and entries made of glass or metal. Access to the chamber and the laser during shots on target is prevented by a dedicated safety system.

The laser irradiance in the study was about 10^{17}–10^{19}, resulting in a Maxwellian distributed electron spectrum with a mean energy of 1.5 MeV. These electrons generate γ-radiation in the target and around the experimental setup. Γ and neutron radiation was measured around the chamber and in the surrounding areas for different laser shot configurations on solid and semi-solid (foam) targets. Table 3.3 lists the different configurations.

Table 3.3: Laser shot configurations for the test series at the LULI 100 TW laser system

Energy [J]	Num. of shots	Target	Thickness [µm]
	15	Teflon	175
14–20[(a)]	25	Al	25
	30	Au	20
< 5	80	Exploded CH	200
20	1	Au	100

[(a)] High-energy configuration

Doses from γ-radiation, expressed as ambient dose equivalents, were measured with TLDs at 50 positions, with two or three dosimeters at each position. After 70 shots with energies of 14–20 J on solid targets, which the authors called the high-energy configuration, some of the TLDs on the experimental chamber were removed. Thereafter followed another 80 shots with lower energy. Photographic films were exposed at some of the positions of the TLDs for comparison. A single shot of 20 J on a 100 µm thick gold foil was used to quantify the γ-dose close to the chamber from a full-power shot on a high-Z target. Ambient neutron dose equivalents from nuclear reactions, (γ,n), were measured with a bubble dosimeter positioned in contact with the chamber, discriminating thermal and fast neutrons. The response of personal dosimeters was also studied, despite the expectation that these would fail due to the extremely short pulses. In addition, activation and contamination measurements were performed by γ spectrometry and wipe tests on the chamber wall and inside parts of the setup.

The dose equivalents obtained from TLD measurements at different positions in contact with the experimental chamber and areas around the experimental set-up are presented in Table 3.4. Shots in the high-energy configuration delivered in general 90–95% of the doses, and the γ-emission peaked in the forward direction, in a 60° cone. The dose behind a 5 cm lead shield was reduced to 0.20 mSv. The doses on top of the chamber were about 7.5 mSv, which is 10 times higher than the doses below it. The results from photographic films and TLDs showed good agreement. Dose equivalents outside the area were all below 100 µSv, except for an area on the next floor, immediately above the chamber where a dose of 450 µSv was measured. It was concluded that measures should be taken to improve radiation safety, in terms of more shielding or prohibiting access to the area. The doses along the beam axis for the total of 150 shots were found to be 50–75 mSv. The mean energy of the γ-emissions was estimated to be 700 keV from attenuation calculations.

Table 3.4: Dose equivalents from γ-radiation at three different locations in contact with the experimental chamber. For surrounding areas, doses are given as the range between different positions. The distance given is from the target inside the experimental chamber.

Measurement position	Distance [m]	TLD γ- dose equivalents [mSv]	
		150 shots all targets	70 shots[(a)] Teflon, Al, Au
Experimental chamber	0.5	49	42
		73	30
		9	8
Experimental area	2.5–7	0.05–0.2	
Adjacent rooms	3–6	0.03–0.1	
Second floor	2–8	0.03–0.5	

[(a)] High-energy configuration

The dose equivalents measured with TLDs and EPDs in contact with the experimental chamber, and neutron doses from bubble dosimeters are given in Table 3.5. Fast neutrons gave the highest dose, of 0.8 mSv, which was still 100 times less than γ-doses at the same position. Doses from fast neutrons were ten times higher than those from thermal neutrons. The EPDs gave no readings, as was expected, due to the short pulses (a few hundred femtoseconds). The measurements for one full-power shot showed a maximum dose of 0.5 mSv in the forward direction. This agreed well with the values of 30–40 mSv for 70 high-energy configuration shots presented above.

Table 3.5: Dose equivalents obtained from TLDs and EPDs, and bubble dosimeters for fast neutrons (n_{fast}) and thermal neutrons ($n_{thermal}$). The distance given is from the target inside the experimental chamber.

Distance (m)	γ-dose equivalents [mSv]		Neutron dose equivalents [mSv]	
	TLD	EPD	n_{fast}	$n_{thermal}$
0.5	40; 45; 82	< 1	0.4; 0.4; 0.8	0.04; 0.05; 0.08
1.2	6.0; 7.4	< 1	0.06; 0.07	0.007; 0.008

The results obtained with γ-spectrometry showed only nuclides from the natural background, and no activation products were identified for the chamber itself, parts of the internal setup, e.g., the target holder, and wipe tests.

The authors compared the dose equivalents determined in this test series with international exposure limits. It was assumed that the normal working conditions over a one-year period would be equivalent to five similar series of shots, i.e., 800 shots per year. Based on this assumption, the dose was found to be below 1 mSv per year, as specified in the ICRP 60 recommendations, at almost all positions. Doses up to 2.5 mSv per year were, however, estimated for working areas on the second floor, above the experimental chamber. The authors therefore deemed it necessary to install adequate biological shielding, or to restrict access to this area during laser operation. The doses within 2 m of the chamber rapidly exceeded the annual exposure dose limit, and it was concluded that the existing radiological classification of the experimental area and access restrictions during shots were justified. Doses from γ and neutron radiation in direct contact with the chamber could exceed 370 mSv and 2 mSv, respectively.

Finally, the authors concluded that their study had led to a quantitative evaluation of the radiological risks associated with different shot configurations, and that the amount of radiation depended on the laser energy and the nature of the target. Based on their findings, they were able to define protection and radiological controls for personnel and different areas of their facility. In addition, they confirmed that ultra-high intensity lasers can generate significant amounts of radiation, and that the radiological safety of personnel must be carefully considered when designing such facilities.

3.3 Petawatt laser systems

Laser–gas and laser–solid interactions

The Extreme Light Infrastructure (ELI), part of the European Strategy Forum on Research Infrastructures, will see the next generation of PW class facilities. It will be the world's largest laser research facility, offering the most intense beamline system worldwide, and the first international user facility in beamline and laser research. Ultra-high intensity interactions will be explored, and radiation sources in an extraordinary energy range are foreseen: electron beams are expected to range between 1 and 50 GeV and protons from 100 MeV up to 3 GeV (Ferrari et al., 2013). The research centers will be placed at four different sites, three of which are: ELI-Beamlines in the Czech Republic, the ELI-Attosecond Light Pulse Source in Hungary, and ELI-NP in Romania. The fourth site is yet to be decided.

A number of studies on radiation protection have been carried out for ELI-NP (e.g., Ferrari et al., 2013a; Ferrari et al., 2013b; Olsovcova et al., 2014a; Popovici et al., 2015; Bechet et al., 2016, Mitu et al., 2016 and Popovici et al., 2017.) The main results of the study by Popovici et al. (2017) are summarized in this section.

In the study entitled: *Shielding Assessment of High Field (QED) Experiments at the ELI-NP 10 PW Laser System*, Popovici et al. (2017) evaluated the bulk shielding that has been constructed for experiments at ELI-NP in Romania. One of the goals of the study was also to investigate compliance with legal dose limits, and to investigate the effectiveness of a beam dump and solutions for muon shielding. The facility will host a high-intensity 2×10 PW laser system and record beam intensities of 10^{23}–10^{24} W cm^{-2} are expected, with energies of about 250 J per shot and a duration of < 20 fs, with up to one shot per minute. The beamlines will produce extremely high-energy γ-rays for different nuclear physics applications.

A completely different radiation environment is expected here, compared to other laser facilities, because of the extremely high power. Particles will be generated at energies above the threshold for electromagnetic and hadronic cascades and pion production. Therefore, the buildings have been designed in line with the principles of radiation protection for conventional high-energy accelerators. A controlled access system will be implemented to prevent any unauthorized or accidental entry during operation, and the room containing the interaction chamber and adjacent zones will be classified as controlled areas. The authors stated that well-documented radiation protection policies and practices have been used in the design of the facility and refer to the study by Fasso and Rokni (2009).

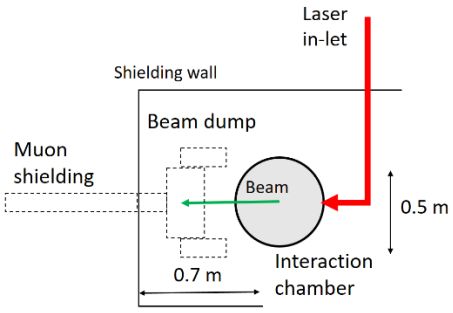

Figure 3.3: Sketch of the experimental area for the ELI-NP 10 PW laser system surrounded by 2 m thick radiological protection walls (fixed concrete walls and movable concrete blocks). The interaction chamber, electron beam dump and muon shielding are indicated. The interaction chamber is made of an aluminum alloy, has 15 cm thick walls and is approximately 4.5 m wide with a height of 2.65 m. The beam dump is made of graphite, copper and tungsten embedded in heavy concrete. The suggested muon shielding has a length of 7 m and is filled with soil.

The shielding assessment was carried out using FLUKA simulations for the experimental area shown in Fig. 3.3, which is expected to yield the highest ambient dose equivalents. The authors claim that the radiation levels are expected to be the highest of all laser facilities worldwide. Early in the ELI project, source terms for different experiments were defined by carefully applying scaling laws and results from particle-in-cell (PIC) calculations. These were used in the building design to ensure adequate radiation protection. The experiments are still being designed, and the source terms are continuously updated and evaluated with regard to radiation protection. The main features of the source terms for five different experimental setups are given in Table 3.6.

Table 3.6: Source terms obtained through FLUKA simulations for specific experimental configurations

Type of experiment		Energy distribution	Divergence	No. of particles per shot
SE1	Electron laser wakefield acceleration	Gaussian, E_{max}= 38 GeV, $\Delta E/E$ = 10%	3°	$1.4 \cdot 10^{10}$
SE2	Electron acc. in overdense plasma	Relativistic Maxwellian, T_{hot} = 116 MeV, cut-off 1.2 GeV	Isotropic	$5.0 \cdot 10^{12}$
SE3	Electron acc. in thick target, 2 mm Au	Similar to SE2	Pencil beam	$5.0 \cdot 10^{12}$
SP1	Proton acc. in radiation pressure or breakout afterburner regimes	Gaussian, E_{max}= 500 MeV, $\Delta E/E$ = 10%	5°	$1.0 \cdot 10^{12}$
SP2	Proton TNSA	Uniform, 100 MeV	40°	$6.0 \cdot 10^{12}$

The total irradiation time was estimated to be 300 minutes per day, 250 days a year, with a laser repetition rate of one shot per minute. These were regarded as reasonable assumptions given that the parameters will be different in each experiment. Dose limits were set at 2 mSv for workers and 0.1 mSv for members of the public. This led

to an average dose equivalent rate of 1 µSv h^{-1} as a conservative design constraint for occupational exposure, and 0.1 µSv h^{-1} for members of the public (assuming the same person is exposed during the total irradiation period). In some less frequently occupied areas, where interlocking systems will be used on doors, rates up to 25 µSv h^{-1} were considered acceptable. These areas were classified as controlled.

Some of the total dose equivalent rates simulated using FLUKA arising from the electron laser wakefield acceleration experiment (SE1) are presented in Table 3.7. The source term, consisting of a 38 GeV electron beam, will generate a bremsstrahlung spectrum extending from zero to the energy of the electrons. The photons produce a range of photonuclear reactions resulting in slow and fast neutrons, protons, muons, pions, kaons, etc., the most difficult of which to shield against are neutrons and muons[2]. Neutrons will be effectively shielded by the room's concrete walls. It has been suggested that a local external muon shield (7 m long) can be built composed of soil, which gives a reasonable balance between protection and cost when additional access restrictions are implemented. It was concluded that the dose rates were within the design dose rate constraints of 1 µSv h^{-1} for areas without access restrictions outside the experimental area.

Table 3.7: Ambient dose equivalents obtained from FLUKA simulations of experiment SE1, a 38 GeV electron beam, and SP1, a 500 MeV proton beam with a Gaussian energy distribution. A maximum repetition rate of 60 shots per hour was assumed. All values are rounded to the nearest power of ten. Positions at the interaction chamber (IC), electron beam dump (BD) and muon shielding (MS) are given relative to the direction of the beam.

Position	Experiment	Before IC	IC	After IC	BD	Behind BD and wall
		[µSv h^{-1}]	[µSv h^{-1}]	[µSv h^{-1}]	[µSv h^{-1}]	[µSv h^{-1}]
Laser beamline	SE1	1–10	$10–10^{6}$	10^{6}	$10–10^{8}$	1–10 [(a)]
	SP1	$10^{2}–10^{3}$	$10^{3}–10^{8}$	10^{8}	$1–10^{8}$	10^{-2}
Roof	SE1	$\leq 10^{-2}$	$\leq 10^{-1}$	$\leq 10^{-2}$	$\leq 10^{-2}$	$\leq 10^{-3}$
	SP1	$10^{-3}–1$	$10^{-3}–1$	$10^{-2}–6\cdot10^{0}$	$10^{-3}–1$	$10^{-3}–10^{-1}$
Basement	SE1	$\leq 10^{-4}$	$\leq 10^{-1}$	$\leq 10^{-1}$	$10^{-3}–10^{-1}$	$< 10^{-4}$
	SP1	10^{-2}	$10^{-4}–1$	$1–2.5\cdot10^{1}$	$1–2.5\cdot10^{1}$	$\leq 10^{-2}$

[(a)] Dose rate mainly due to muons

The equivalent dose maps obtained from the experiments on laser acceleration in thick targets (SE2 and SE3) for which the energy distributions and number of particles were similar (T_{hot} = 116 MeV, cut-off 1.2 GeV) but different beam divergence (isotropic vs. pencil beam), showed contrasting and very different spatial distributions. The authors attributed this to the influence of the experimental setup on the spatial dose distributions, despite the fact that similar particle energies are involved.

The strongest proton source term considered in the simulations arose from the SP1 experimental set-up (Table 3.6). The secondary particles will be created by inelastic interactions between the primary proton beam and the surrounding material, which will be followed by electromagnetic cascading. Different nuclear processes, e.g.,

[2] The photon energy threshold for muon pair production is 211 MeV. Muons are also produced in the decay of pions.

fission and evaporation, will produce secondary neutrons, protons, pions, kaons, heavy fragments and γ-rays. Table 3.7 also presents a selection of the authors' FLUKA results for ambient dose equivalents.

The design dose constraints were not met at two locations; on the roof and in the basement, by factors of 6 and 25, respectively. A higher neutron fluence was seen here than with the SE1 experiment. The authors stated that these areas will be continuously monitored, and if elevated dose rates are found, the laser shot repetition rate could be decreased. Additional neutron shielding could also be added.

The aim of the SP2 experiment is to produce energies at the upper limit of previously reported TNSA experiments. The ambient dose equivalent rates were mostly within the design dose constraints, although there were some exceptions. The same reasoning was applied as in the previous case, i.e., that the laser shot rate could be reduced if elevated values were recorded. In addition, the access control system will prohibit occupancy of these areas during laser operation.

The authors concluded that the main types of ionizing radiation that will escape the shielding around the experimental area will be γ-rays and neutrons. Appropriate detectors should therefore be chosen to monitor the relevant radiation characteristics. The authors proposed two types of detectors: one for residual activity measurements positioned inside the experimental area, operating only when the laser beam is off, and another for pulsed field measurements positioned outside the experimental area and is always on. These detectors are described in more detail in the reports by Mitu et al. (2016) and Cernaianu et al. (2016).

It was also concluded that during experiments, the radiation fields around the interaction chamber will significantly exceed the relevant dose limits, and that a controlled access system will be necessary. Existing shielding was deemed to be sufficient except in the case of muons, which constituted the main radiation protection issue, and could escape from the experimental building. A local muon shield with appropriate dimensions and composition was therefore suggested.

3.4 Further reading

Additional studies on radiation protection and the characterization of radiation fields around high-intensity lasers are listed in Table 3.8, categorized according to laser power and type of interaction.

Table 3.8: Selected studies on radiation protection and radiation field characterization around high-intensity laser facilities. *The articles are also listed in the reference section.*

Laser power	Interaction	Paper
Gigawatt	Laser–solid	Fonseca et al. (2010). *High electron doses from a GW laser interacting with solid aluminum targets*
		Fonseca et al. (2010). *Measurement of radiation produced by ultra-short laser pulses interacting with solid targets*
Terawatt	Laser–gas	Lefebvre et al. (2003). *Electron and photon production from relativistic laser-plasma interactions*
		Esposito (2011). *Radiation protection issues for laser-based accelerators*
		Olsovcova et al. (2014). *Response of dosimeters in the radiation field generated by a TW-class laser system*
		Olsovcova et al. (2014). *Radiation protection aspects in the vicinity of TW class laser systems*
		Strand Berg, J. (2016). *Monte Carlo simulations and measurements of the radiation environment at a laser-plasma accelerator*. Master thesis
		Bauer et al. (2017). *Ionizing Radiation from Terawatt Lasers at SLAC*
		Yang et al. (2017). *Dosimetric evaluation of laser-driven X-ray and neutron sources utilizing XG-III ps laser with peak power of 300 terawatt*
	Laser–solid	Borne et al. (2002). *Radiation protection for an ultra-high intensity laser*
		Hayashi et al. (2006). *Estimation of photon dose generated by a short pulse high power laser*
		Qiu et al. (2011). *Analysis and mitigation of X-ray hazard generated from high intensity laser–target interactions*
		Olsovcova et al. (2014). *Response of dosemeters in the radiation field generated by a TW-class laser system*
		Liang et al. (2015). *Measurements of High-Intensity Laser Induced Ionising Radiation at SLAC*
		Florescu and Duliu (2016). *Shielding activation of petawatt laser facilities in Romania: a FLUKA preliminary evaluation*
		Liang et al. (2016). *Radiation Dose Measurements for high-intensity laser interactions with solid targets at SLAC*
		Bauer et al. (2017). *Ionizing Radiation from Terawatt Lasers at SLAC*
		Liang (2017). *Characterization of Ionizing Radiation Generated from Interaction of High-Intensity Laser with Matter*. Doctoral dissertation
		Liang et al. (2017). *Bremsstrahlung dose yield for high-intensity short-pulse laser–solid experiments*
		Yang et al. (2017). *Dosimetric evaluation of laser-driven X-ray and neutron sources utilizing XG-III ps laser with peak power of 300 terawatt*
		Yang et al. (2017). *Photon dose estimation from ultraintense laser–solid interactions and shielding calculation with Monte Carlo simulation*
		Yang et al. (2017). *Measurements of X-ray doses and spectra produced by picosecond laser-irradiated solid targets*

Table 3.8: (Continued)

Laser power	Interaction	Paper
Petawatt	Laser–gas	Olsovcova et al. (2014). *Bulk shielding for laser research centre ELI Beamlines*
		Popovici et al. (2015). *Preliminary dosimetric evaluation of electron source terms at PW laser systems*
		Mitu et al. (2016). *Radiation protection and safety at ELI–NP*
		Florescu et al. (2017). *Radiological safety assessment for the experimental area of a hyper-intense laser with peak—power of 1PW—CETAL*
		Popovici et al. (2017). *Shielding assessment of high field (QED) experiments at the ELI-NP 10PW laser system*
	Laser–solid	Allott et al. (2000). *Vulcan Petawatt Upgrade: The Radiological Perspective*. Annual Report 1999/2000, Rutherford Appleton Laboratory, UK.
		Clarke et al. (2006). *Radiological characterisation of photon radiation from ultra-high-intensity laser-plasma and nuclear interactions*
		Ferrari et al. (2013). *Radiation field characterization and shielding studies for the ELI Beamlines facility*
		Ferrari et al. (2013). *Radiation field characterization and shielding studies*
		Clarke et al. (2014). *Proton activation history on the Vulcan high-intensity petawatt laser facility*
		Olsovcova et al. (2014). *Bulk shielding for laser research centre ELI Beamlines*
		Popovici et al. (2015). *Preliminary dosimetric evaluation of electron source terms at PW laser systems*
		Bechet et al. (2016). *Radiation protection of a proton beamline at ELI-Beamlines*
		Mitu et al. (2016). *Radiation protection and safety at ELI–NP*
		Florescu et al. (2017). *Radiological safety assessment for the experimental area of a hyper-intense laser with peak—power of 1PW—CETAL*
		Popovici et al. (2017). *Shielding assessment of high field (QED) experiments at the ELI-NP 10PW laser system*

4 Modelling the radiation environment

A valuable starting procedure to characterizing the radiation at a facility is to perform simulations. This is also crucial at the planning stage for constructing new facilities to dimension shielding and develop radiation safety protocols for which no measurements can be made.

Radiation protection/shielding simulations are mainly based on Monte-Carlo codes and have been reported to be very accurate, e.g. by Battistoni et al. (2007) in “The FLUKA code: description and benchmarking”.

4.1 Monte Carlo codes

Monte Carlo methods take a statistical approach on studying equations and were for a time mainly used to study stochastic problems (i.e. problems that are intrinsically random). The simplest way of explaining a Monte Carlo method is as a process to estimate the parameters of a certain distribution. In reality it is more correct to say an estimation of a function describing the parameter as there is some uncertainty. In ”Monte Carlo Methods for Radiation Transport”, Vassiliev (2017), the general scheme for solving a problem using Monte Carlo methods is stated as:

1. Develop a mathematical model of the physical problem.
2. Formulate a statistical interpretation of the model, expressing the quantity of interest as a parameter belonging to a distribution.
3. Develop an algorithm for sampling the distribution.
4. Derive estimators for the parameters along with its statistical uncertainty.
5. Implement variance reduction methods. That is, methods that reach the desired statistical uncertainty within reasonable computation times.
6. Generate a sample large enough to reach the desired uncertainty in the parameter estimation. In the case of Monte Carlo particle transport codes, this corresponds to generating a sufficiently large number of particles.
7. Estimate the parameter and its uncertainty using the sample.

As the Monte Carlo method is widely used for the purpose of simulating particle transport and interaction, there is a variety of codes available for this purpose. What follows here is a brief overview of the most commonly used codes.

FLUKA

FLUKA is a general-purpose Monte Carlo code that simulates the interaction and transport of hadrons, heavy ions and electromagnetic particles developed by the European Organization for Nuclear Research (CERN) and the Italian Institute for Nuclear Physics. FLUKA includes all the necessary physics for radiation protection purposes, such as hadronic and nuclear interactions and hadronic and electromagnetic interactions.

FLUKA is written in Fortran and also supports parallel computing, making it a computationally fast code. A comprehensive overview of the FLUKA code was

presented in “The FLUKA Code: An Accurate Simulation Tool for Particle Therapy”, by Battistoni et al (2016).

FLUKA can also be used via a powerful graphical user interface called FLAIR, developed by V. Vlachoudis (2009). This enables the use of FLUKA with minimal coding and one can work explicitly with the user interface for simpler problems. However, the possibility to write user defined routines is still available for the more advanced user.

GEANT4

GEANT4 is an object-oriented toolkit, written in C++, simulating the passage of particles through matter and has been used within many areas of application. It is a very flexible toolkit that allow users to write their own application but it is also more complex than some codes. GEANT4 supports multithreading which has recently been added and several improvements and extensions are planned for future updates, mentioned in “Recent developments in GEANT4”, Allison et al. (2016). GEANT4 is modular, as the user decides which physics are to be included in the current model, allowing for optimization. For radiation protection purposes, all the necessary physics are available at a broad range of energies.

MARS15

MARS15 is a Monte Carlo code used for shielding, accelerator design and detector studies. It simulates detailed hadronic and electromagnetic cascades in arbitrary 3D geometries and is valid in energies up to 100 TeV. It has been developed for over 30 years at the Institute of High Energy Physics, Superconducting Super Collider Laboratory and Fermilab and it also includes a user-friendly interface for visualization of geometry, materials, fields and other results.

MCNPX

This is a general-purpose Monte Carlo code and is an extension of the MCNP code, used for neutron interaction and transport. It now includes almost all particle types and is used within a number of areas such as shielding, accelerator design and medical physics. The code is in Fortran/C and allows for parallel computing.

PHITS

This was one of the first codes to simulate transport and interactions of heavy ions and is based on NMTC/JAM, a high-energy hadron transport code. It now contains all particles and is capable of accurately simulating interactions at energies up to 200 GeV (for hadrons) and is written in Fortran. It contains several physics models for a variety of interactions, such as INC-ELF, BERTINI and GEM. A more detailed description of PHITS can be found in “Development of General-Purpose Particle and Heavy Ion Transport Monte Carlo Code”, by Iwase et al. (2002).

4.2 Radiation fields at the LLC

This work was carried out using FLUKA with the purpose of characterizing the radiation environment at the LLC. This actually constitutes of two accelerators, one of which is a laser wakefield accelerator (LWFA), accelerating electrons to an average energy of 120 MeV. The other is a plasma accelerator based on TNSA and accelerates protons to energies of a few MeV, along with some electrons.

FLUKA includes most of the required physics by default and was run in "PRECISION" mode. This means that:

- Electromagnetic field interactions are included.
- Rayleigh scattering and inelastic form factor corrections to Compton scattering and Compton profiles are activated.
- Detailed photoelectric edge treatment and fluorescence photons are activated.
- Low energy neutron transport on down to thermal energies is included, (high energy neutron threshold at 20 MeV).
- Complete analogue absorption for low-energy neutrons is activated.
- Particle transport threshold is set at 100 keV, except neutrons (10^{-5} eV), and (anti)neutrinos.
- Multiple scattering threshold at minimum allowed energy is activated, for both primary and secondary charged particles.
- Delta ray (secondary electron) production is included with a threshold at 100 keV.
- Restricted ionization fluctuations are included, for both hadrons/muons and electromagnetic particles.
- Tabulation ratio for hadron/muon dp/dx is set at 1.04. The fraction of kinetic energy to be lost in a step is set at 0.05. Number of dp/dx tabulation points is set at 80.
- Heavy particle e+/e- pair production is activated with full explicit production (with the minimum threshold = 2 ·electron mass).
- Heavy particle bremsstrahlung is activated with explicit photon production above 300 keV.
- Muon photonuclear interactions are activated with explicit generation of secondaries.
- Heavy fragment transport is activated.

Further, photonuclear interactions were included by adding the corresponding card[3].

The scored[4] quantity was chosen to be ambient dose equivalent, with weight factors from "Conversion Coefficients for use in Radiological Protection against External Radiation", ICPR (1996) and M. Pelliccioni (1998). The total ambient dose equivalent was categorized into different particle types, i.e. beta, gamma and neutron radiation. In the case of proton acceleration, another category was added for protons. This was done by using an "AUXSCORE" card that filters the scoring, each card only scores radiation from the specified particle. This was combined with a 3D Cartesian mesh, having 200 bins in each dimension where the dose was scored, created using a "USRBIN" card.

FLAIR has an option to plot the results directly, using gnuplot. In this case, some post-processing was needed so a MATLAB script was written to import the data acquired from FLUKA. If this is required one has to first export the data as ASCII to make them readable (as the primary results are stored in binary files), this was done for both the geometry and dose data.

The geometric model was done in FLAIR using Geoviewer and figure 4.1 shows a top-down view of the facility as it was implemented in FLAIR. Target 1 corresponds

[3] A "card" refers to a section of code in FLUKA, it stems from the old programming languages (such as Fortran) which used punched, physical cards to store the programs.

[4] Scoring refers to measuring a quantity in FLUKA via a virtual detector.

to the TNSA acceleration room and target 2 is the electron acceleration room. Figure 4.1 also shows the location of a few measurement points presented in table 4.1.

Laser Wakefield Acceleration

As it is a pulsed radiation source, one has to make an estimation on the annual average number of shots to obtain a yearly dose. The number of accelerated particles also fluctuate from shot-to-shot, demanding an estimation of this number as well.

In the simulations presented here, an average number of accelerated particles was assumed to be $2 \cdot 10^8$ electrons per shot (32 pC), based on previous measurements (O. Lundh et al. 2012). Further, the electron beam has an average energy of 120 MeV, a Gaussian energy distribution with a standard deviation of 30 % (equivalent to a momentum spread of 0.02 GeV/c) and a half angle divergence of 3 mrad (O. Lundh et al. 2012). The electron distribution in the beam (perpendicular to its propagation, i.e. the spot size) is Gaussian with a full width at half maximum (FWHM) of 2.5 µm (horizontal) and 3.4 µm (vertical) approximately (K. Svendsen, 2017). The number of shots taken during a year at the facility is something that depends on the campaigns and experiments performed during this time. An estimated average was taken as 30,000 shots during one year for electron acceleration.

Target Normal Sheath Acceleration

TNSA creates a very special source that cannot be handled by any defaults in FLUKA. Therefore, a user defined source file was created to be given as input to FLUKA when generating particles. This code creates both electrons and protons, half of them propagating in the laser direction and the other half propagating in the opposite direction. This is an assumption as the back-propagating beam has never been measured at LLC. The majority of papers on the subject has observed slightly less energetic protons in the backwards direction and in "TNSA in the ultra-high contrast regime" by Ceccotti (2008), 2D PIC simulations show very similar proton spectra in both directions, except a lower maximum energy in the backwards direction. Hence, a worst-case scenario (in a radiation protection sense) would be having the forward spectrum also in the backwards direction, which was used in these simulations.

The divergence is large and energy dependent, which in turn depends on the sheath formation, a parabolic sheath results in a more parabolic energy dependence. A flat sheath gives a linear relation between energy and divergence, reaching a half opening angle of 21 degrees (Ion Acceleration - Target Normal Sheath Acceleration, Roth and Schollmeier (2013)). In these simulations, it was assumed to be linear, the sheath formation is not known but the parabolic dependency exhibits itself mostly at the highest energies and is semi-linear at moderate energies.

The energy spectrum for the protons was taken from measured data and converted to a probability distribution, which was used to sample particle energy. The proton energy spectrum has a cut-of energy as they are dispersed by a dipole magnet. Lower energy protons are deflected at a larger angle and does not enter the aperture sitting in front of the scintillator, thus they are not detected so the spectrum only goes down to 1 MeV. The maximum proton energy is at 5 MeV, for this reason all generated protons have an energy between these values, following the measured distribution. Protons at higher energies have been detected at LLC, up to 10 MeV, but as the spectrum is highly exponential these will not be observed unless the statistical sampling pool is very large. By this reasoning, the end result would marginally change by extrapolating the spectrum and this was deemed unnecessary as the higher energy protons are a rare observation.

During TNSA, both hot and cold electrons are generated. The cold electrons were neglected in these simulations as they have a relatively low energy compared to the hot electrons. The hot electrons reach higher energies due to the ponderomotive force exerted by the laser. There exist a few different scaling laws for determining the hot electron temperature, the most recent one being Haines' scaling (Haines et al., 2009). This was used to calculate the hot electron temperature which for the current laser parameters (intensity of $2 \cdot 10^{19}\,\mathrm{W/cm^2}$ and a wavelength at 800 nm) gives a temperature of 0.67 MeV. The spectrum is in turn assumed to follow a Maxwell-Boltzmann distribution (B.Yang et al. (2016)).

From previous measurements at LLC, the proton yield is known to be on the order of $10^{11}\,\mathrm{protons/MeV/sr}$ at 1 MeV and the conversion efficiency from electron to proton energy has been reported to be 4–9% (O. Lundh 2008). In this case, it was assumed to be 5% which at LLC is the upper limit. For the hot electrons, which accelerate the protons, the conversion efficiency from the laser energy is roughly 20% (Senje 2017). This means that 20% of the laser energy is converted to electrons, 5% of the electron energy is then further converted to protons, resulting in an electron-proton ratio of 3 to 1. Note that this assumes that the electron and proton spectrums have the same temperature and distribution.

Similarly, as for the electron acceleration case, an estimation was made on the number of shots taken each year. This was stated to be 2,000 on average and in each shot $2 \cdot 10^{12}$ particles (electrons and protons) are accelerated, 33 % of which are protons. Half of these particles (protons and electrons) are accelerated in the forward direction and the other half in the backwards direction, as stated before.

FLUKA results - Radiation environment

Figure 4.2–4.4 shows the calculated ambient dose equivalent obtained in FLUKA with values in mSv/pC for each particle type (electron, photon and neutron), note that the color bar has logarithmic values. From this it can be concluded that the beta radiation from LWFA is highly directed towards the back of the room and while the gamma radiation follows this pattern, it penetrates and spread farther. Some neutrons are generated via LWFA but it is a fairly low quantity. From TNSA, neither electrons nor protons have enough energy to escape the vacuum chamber and no neutrons are generated. The main contribution to the radiation field from TNSA is thus gamma radiation that expands in the forward and backward direction of the beam.

Figure 4.5 shows the total ambient dose equivalent for all particle types in mSv/pC. A typical shot contains approximately 32 pC of charge (for LWFA) by which the maximum ambient dose equivalent for a single shot is 7.8 µSv, located just where the beam exits the chamber. This is a rather small dose, on par with the daily background radiation dose received by an average person (6 µSv). As a conclusion, LWFA generates most of the radiation per charge but since TNSA generates a lot more charge, the contribution from TNSA becomes significant.

The annual ambient dose equivalent is shown in figure 4.6 with values in mSv/year. Here it can be seen that the TNSA source gives higher values compared to previous figures in relation to LWFA, this is due to the large number of particles accelerated in each shot, $2 \cdot 10^{12}$, compared to $2 \cdot 10^{8}$ particles for LWFA. To obtain the annual ambient dose equivalent it was assumed that 2,000 TNSA shots were taken, along with 30,000 LWFA over a year. Figure 4.7 shows the transversal annual ambient dose equivalent with the main purpose of examining the radiation reaching the office space located above target 1. As a conclusion, the dose is less than 1 nSv/year with the

exception of a few stray neutrons which increase this value to approximately 10 nSv/year at a few locations.

According to the current safety protocols, all personnel must be behind the lead wall when either accelerator is in operation, looking at figure 4.6, the ambient dose equivalent is on the order of 1 µSv/year at this location, well within the limit of 6 mSv/year. One needs to keep in mind that this assumes a certain number of shots and it scales linearly. Therefore, one can estimate a "shot limit" to not exceed the recommended dose limits. This is especially important if the repetition rate of the system changes. If the system goes from 1 Hz to 1 kHz, more shots will be possible in the same time limit and if this is fully utilized the dose will also increase a factor 1000. According to these simulations, the main contribution to the ambient dose equivalent behind the lead wall comes from TNSA. This gives a shot limit for TNSA of $12 \cdot 10^6$ shots / year, which is 6000 times more than the average yearly shot number today.

Comparison with measured dose

Three detectors are permanently placed in the lab and checked each month. However, it is difficult to compare the simulated values (figure 4.6) to these as the setups and environment in the lab is constantly changing. The number of shots is also something that may vary greatly from time to time for both LWFA and TNSA. Further, all simulated values at the TLD locations are much smaller than the natural background radiation, making any comparison obsolete. One statement is true however, the generated radiation at these locations are below the natural background radiation, which the simulation confirms. Table 4.1 shows the total readout values for the TLDs over a year along with the simulated values at this locations, including values at additional key locations, marked in the layout (figure 4.1).

The TLD sitting next to the door leading to the hallway (T3), behind the lead wall shows a value of 1.5 mSv/year. The detector shows a higher value than the simulations and a higher value than the detector in the beam direction. The experimental room was built many years after the main building so the inner walls in this room are newer. The old wall (separating the hallway and the experimental room) is from the original building and is a different type of concrete, possibly even blue concrete that contains uranium and emits gamma radiation. This suspicion was strengthened as a measurement with a Geiger counter showed levels of 1.2-1.6 µSv/h from the old walls and the new walls showed 0.9 µSv/h. A dose rate difference of 0.3 µSv/h will over a year accumulate to 2.6 mSv/year. This may explain the high value from this TLD and it has been recommended to move it to a different position.

To further expand this study, one should take into account that, if the laser parameters change, this may influence the behavior of the accelerators and if the laser energy is increased the electron energy from LWFA will also increase. Thus, one may also desire to find a critical electron energy, at which the ambient dose equivalent becomes an issue. The same is true for TNSA and both accelerators should be simulated at higher energies for a more complete study.

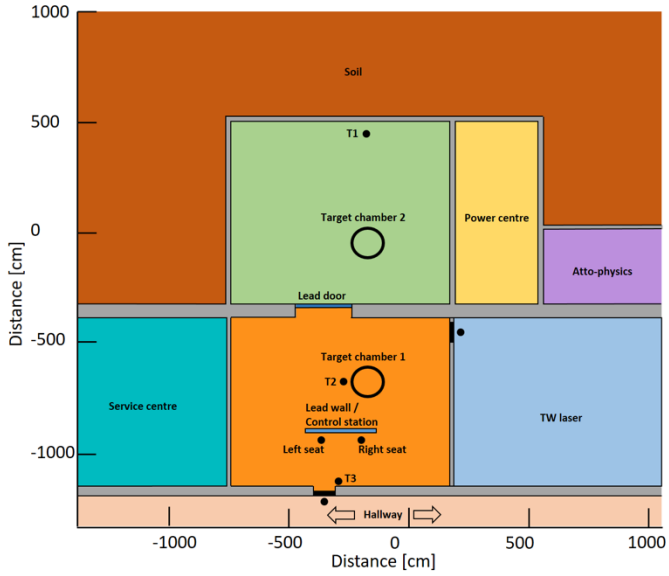

Figure 4.1. Schematic layout of the LLC geometry implemented in FLUKA. Target chamber 1 is where TNSA takes place while the LWFA is located at target chamber 2. A lead door separates the two rooms and the control station is protected by a lead wall. Black dots indicate position of point values given in table 4.1, including the location of three permanently mounted TLDs (T1-T3). The TLD T1 is mounted in the forward direction of the beam (though the beam is redirected using a dipole magnet) and TLD T2 is located in the ceiling above target chamber 1. The third TLD, T3, is mounted directly on the wall next to the door leading to the hallway.

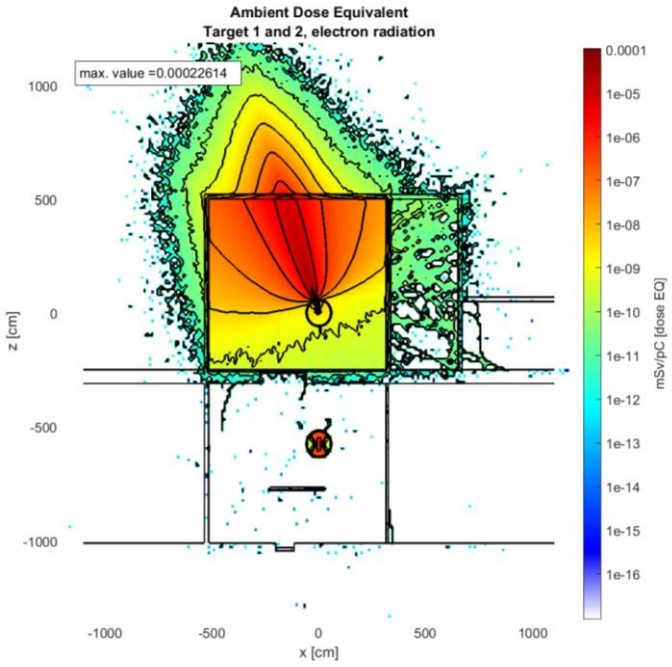

Figure 4.2. The ambient dose equivalent due to beta radiation only, for both LWFA and TNSA, given as mSv/pC. Note that TNSA generates much more charge than LWFA and these values scale accordingly. The beta radiation from LWFA is highly directed and slightly deflected due to the dipole magnet used to disperse the electrons on a scintillating screen. In target chamber 1 (TNSA) the electrons do not have enough energy to penetrate the chamber walls to any significant extent.

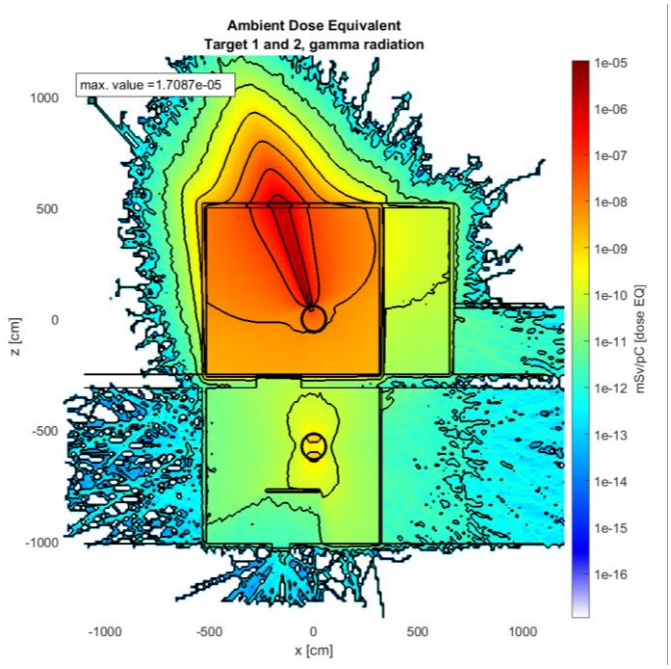

Figure 4.3. The ambient dose equivalent due to gamma radiation only, for both LWFA and TNSA, given as mSv/pC. Note that TNSA generates much more charge than LWFA and these values will scale accordingly. The gamma radiation from LWFA is also highly directed and slightly deflected as most of the gamma radiation is generated as bremsstrahlung from the electrons. As TNSA accelerates particles in both directions, the gamma radiation follows this distribution as well. The lead wall stops a portion of the radiation, approximately one order of magnitude, while the lead door stops about three orders of magnitude.

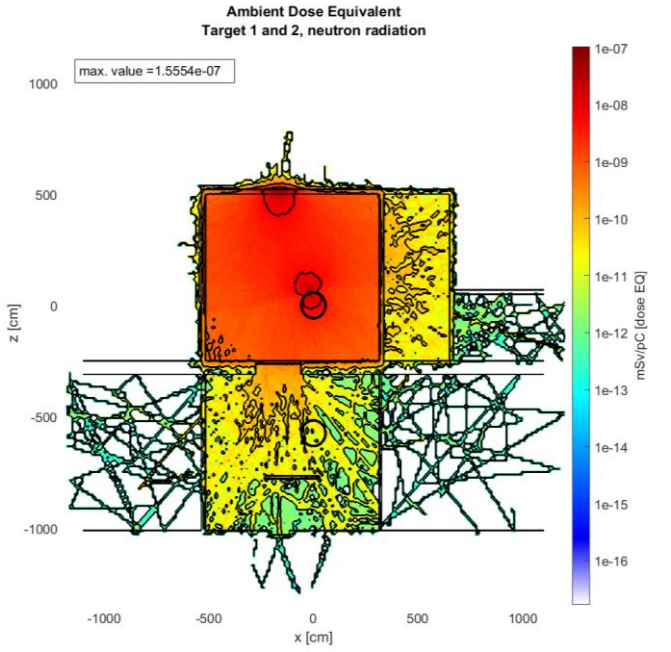

Figure 4.4. The ambient dose equivalent due to neutron radiation only, for both LWFA and TNSA, given as mSv/pC. The source to all neutron radiation is LWFA as TNSA generates less energetic particles. Due to this fact, any source of induced radioactivity will be generated by LWFA.

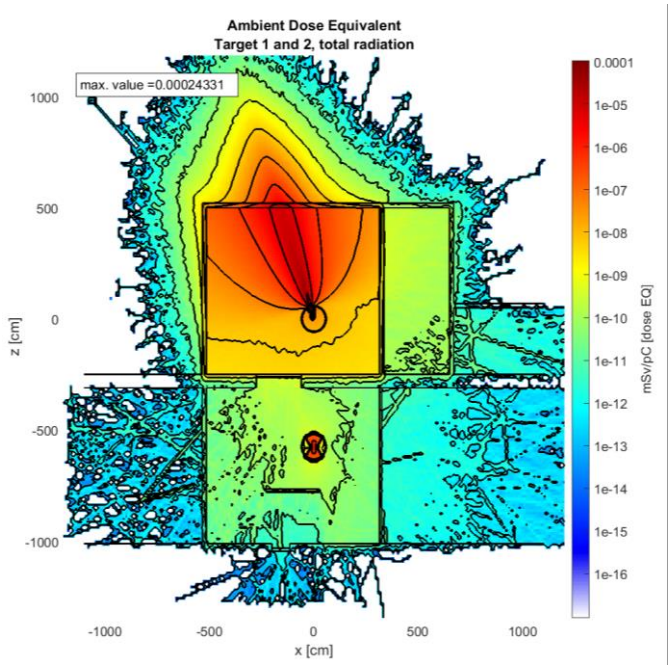

Figure 4.5. The total ambient dose equivalent (all types combined), for both LWFA and TNSA, given as mSv/pC. Note that TNSA generates much more charge than LWFA and these values will scale accordingly. A single shot with LWFA generates approximately $2 \cdot 10^8$ electrons while TNSA generates $2 \cdot 10^{12}$ electrons and protons (on average).

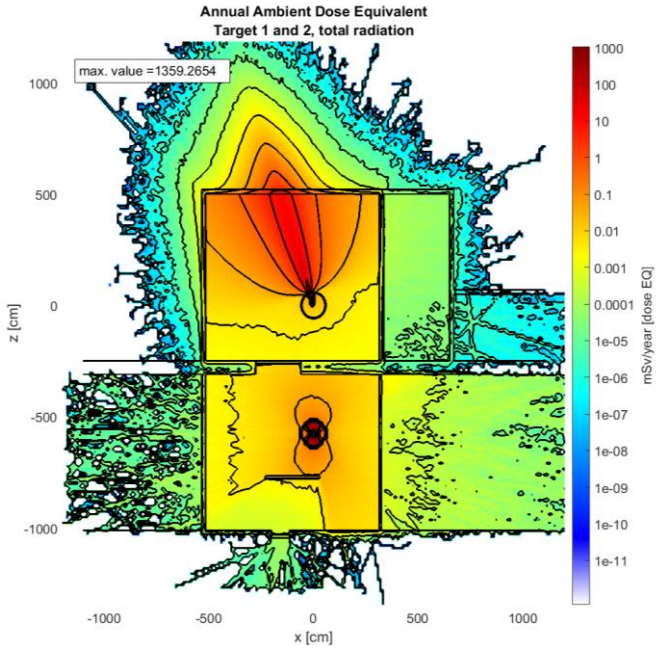

Figure 4.6. Annual total ambient dose equivalent, given as mSv/year for both LWFA and TNSA. This is assuming 2,000 shots for TNSA and 30,000 shots for LWFA over a year, each LWFA shot having a charge of 32 pC and each TNSA shot having a total charge of 320,000 pC. From this it can be concluded that all areas are within the dose limit of 6 mSv/year except in the electron beam direction at target chamber 2 and inside target chamber 1. None of these areas are accessible during operation.

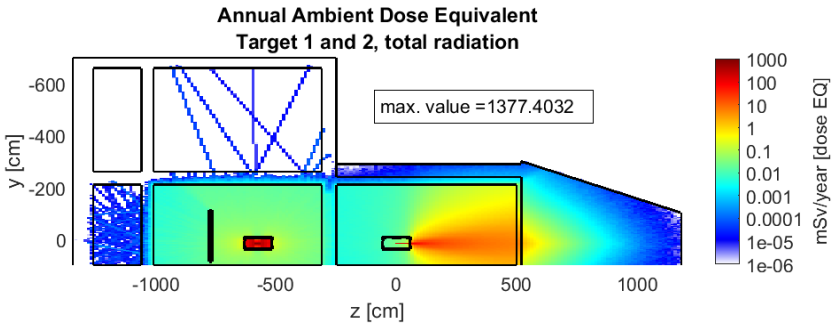

Figure 4.7. A vertical view of the ambient dose equivalent for both target rooms. The bottom left room is the hallway, next to that is target 1, including the control station. The office space located above target chamber 1 has an annual ambient dose equivalent below $1 \cdot 10^{-11}$ mSv/year (truncated here for better visibility) except some stray neutrons.

Table 4.1. Simulated ambient dose equivalent values for certain key locations, see figure 4.1 for the exact locations (indicated by black dots), along with TLD measurements (daily background of 6 µSv). Despite the good agreement one should keep in mind that the reported values are very small, below the level of background radiation, and the accuracy of the measurements may not be adequate. One can still conclude that the levels are below background radiation for both the TLD measurements and the simulated values.

Location	Dose, FLUKA [mSv]	Dose, TLD May 2016- April 2017 [mSv]
Hallway door (T3)	0.0027	1.5
Roof (T2)	0.096	0.1
Beam (T1)	1.078	1
Hallway (by the door)	0.00017	-
Control left seat	0.0070	-
Control right seat	0.0094	-
Hallway	0.00030	-
TW room	0.0072	-

Induced radioactivity

The activation of a previously stable material stems from mainly two processes. One is photodisintegration where a nucleus absorbs a high-energy photon (several MeV) and emits a neutron. The other process is via neutron activation, which is also the most common form of induced radioactivity. This occurs whenever a nucleus captures a free neutron and as such, thermal neutrons have a higher probability to be captured than higher energy neutrons. As TNSA generates close to zero neutrons, only LWFA is of interest in this regard.

Using FLUKA, it is possible to simulate the induced radioactivity. This is done by choosing a radiation time, which was set to 10 fs, generating $8 \cdot 10^{22}$ electrons/s, corresponding to a single shot. This will activate some materials and may be scored in certain regions or in all regions. In this study, all regions were simultaneously studied, observing the total activation. The obtained quantity is residual nuclei per accelerated particle, or Bq at specified time stamps if decay times are included. Since

the induced radioactivity strongly depends on the types of material, a grid of different materials was included inside the target chamber to get an overview of possible elements. These included silicon, silver, copper, iron, lead, tantalum, polymethyl methacrylate (PMMA) and beryllium.

Figure 4.8 and 4.9 shows the activity at two different times, t=0 and t=10 s for a single shot. Just after a shot (t=0) the highest value is for the isotope ^{12}B, having an activity of 10,000 Bq. This is approximately double the activity of the natural potassium content in the human body. 10 seconds after a shot, figure 4.9, some of the short-lived isotopes have decayed completely (^{12}N and ^{12}B) and the maximum activity is due to ^{34}Cl, having a value of 4 Bq.

From these results, one may conclude that there is no notable induced radioactivity for a single shot. To further expand on this study, the induced activity should be simulated for longer periods of time as one may have an accumulation of more long-lived isotopes which may result in a higher activity. This is mostly important for all permanent materials, such as the aluminum chamber and the concrete walls (permanent in that they will be present for every shot).

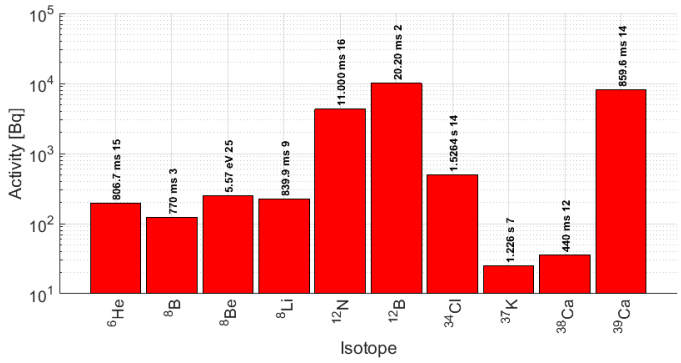

Figure 4.8. The induced radioactivity just after a shot (t=0). The highest activity is due to the isotope ^{12}B, most likely due to the carbon content in the concrete. One should keep in mind that Bq is a very small unit, as a comparison it may be mentioned that the natural potassium content in the human body generates 5,700 Bq. As such, this would be approximately equivalent to standing next to two persons.

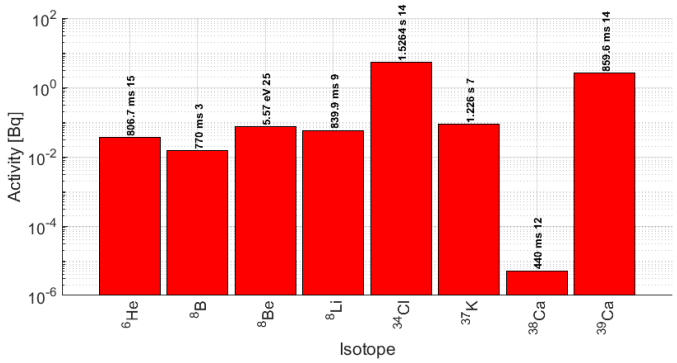

Figure 4.9. The induced radioactivity 10 seconds after a shot. Some of the more short-lived isotopes have fully decayed, such as ^{12}N and ^{12}B. The highest activity is now due to ^{34}Cl at 4 Bq.

Particle-in-cell codes

Monte Carlo codes such as FLUKA are well suited to simulate the radiation environment. In these codes, the source of radiation always has to be defined. This is all well when one has experimental or analytical data to define the source but there might be a situation where this is not possible for plasma-accelerators. In these cases, one might want to also simulate the acceleration process that defines the source, especially if a new facility is being built, for dimensioning radiation shielding and other safety regulations.

The plasma dynamics that govern the acceleration of particles in a plasma-accelerator require sophisticated and computationally demanding numerical models. Numerical modelling of plasma acceleration in the regimes currently explored in the experiments requires a kinetic description of the plasma. The Particle-in-Cell (PIC) technique is a well-established method to solve the Vlasov equations coupled with the Maxwell equations. Fully electromagnetic-relativistic PIC codes provide detailed information about the laser– and beam-plasma interaction, and they constitute nowadays the most powerful method to study this problem.

The resolution of these simulations is limited by the number of particles and the size of the mesh in the plasma, which is further limited by the simulation time as a greater number of particles takes longer to simulate and memory restrictions. These simulations are in general very demanding and require tens of thousands to millions of computational hours on a single CPU (Ekerfelt 2015). For this reason, PIC simulations are performed on data clusters, containing many CPUs, to obtain manageable simulation times.

5 Dosimetry and detector performance

Dosimetry at laser-plasma accelerators is a challenge due to the complexity of the radiation fields which, in ultra-short mode, contain many components with high instantaneous fluxes and dose rates. One difficulty lies in the fact that the secondary radiation field will be composed of a combination of different types of radiation and energies following interactions of the primary beam with the surrounding materials, including shielding. According to the National Council on Radiation Protection and Measurements (NCRP), the range of energies encountered in particle accelerator fields is only found in one other branch of radiation physics, namely dosimetry during space missions (NCRP, 2003). The influence of the pulsed mode on dosimetry is another important issue. Such problems can generally be disregarded at workplaces where ionizing radiation is emitted continuously, and the instruments used to determine exposure are not primarily intended for use with pulsed beams. However, most dosimetry techniques used to measure continuous radiation can also be used for pulsed radiation, provided certain *precautions* are taken e.g., calibration constants appropriate for pulsed beams are used and pulse lengthening is considered. Knowledge obtained from dosimetry at other particle accelerators, also operating in ultra-short pulsed mode, such as linear accelerators and synchrotrons, whose pulses can range from nanoseconds to microseconds with a repetition rate of milliseconds, can also be used. Some accelerators deliver a series of particle bunches during a microsecond, where each bunch can be on the order of picoseconds long, which is similar to laser-plasma accelerators deliver.

The most extensive source of information on dosimetry for pulsed radiation in the form of X-ray and electron beams is provided by the International Commission on Radiation Units and Measurements (ICRU) in Report 34 (ICRU, 1982). High-LET[5] radiation is shortly mentioned and deals mainly with heavy charged particles and neutrons. The report reviews the literature and guides to the most accurate and appropriate measurement system for a particular pulsed radiation and on any precautions necessary to take. Four different dosimetry systems are considered separately: ionization chambers, chemical dosimeters, calorimeters and solid state dosimeters.

A more recent publication on radiological protection issues at particle accelerators is NCRP Report No. 144 (NCRP, 2003). This constitutes a significant revision and expansion of NCRP Report No. 51, originally published in 1977. The report from 2003 includes the significant experience obtained over the intervening period. Updated information is given on source intensities, shielding, dosimetry, and the environmental aspects of particle accelerator operation, and radiological safety aspects that are unique to particle accelerators from 5 MeV up to the highest energies are discussed. One chapter is dedicated solely to techniques for radiation measurements at high-energy accelerators, and discusses the radiation fields that can be expected in such cases. The practical dosimetric techniques available are reviewed, and the problems of dosimetry in pulsed radiation fields are treated in detail.

The European Commission has funded a three-year project (2005–2007) called CONRAD, COordinated Network for RAdiation Dosimetry, which has resulted in a

[5] Linear energy transfer (LET) describes how much energy a particle transfers to the material per unit distance.

report that reviews the techniques and instrumentation relevant for monitoring neutron and photon fields around high-energy accelerators (Bilski et al., 2006). The influence of the pulsed nature of the radiation on its measurement and problems regarding the calibration of devices for high-energy radiation are also addressed. Particularly interesting is the fact that the major high-energy European accelerator facilities are reviewed, together with the organization of workplace monitoring at each facility.

Radiation protection at accelerator facilities is concerned with secondary radiation outside dedicated shielding, while instrument response is usually investigated with regard to primary beam dosimetry. The guidelines from studies on primary beam dosimetry can be applied when taking into account the fact that secondary fields at accelerator facilities are often composed of other types of radiation distributed over a broader energy range, and that the dose rate is lower. In addition, after passing through shielding it is likely that the initial pulse structure will be considerably distorted due to so-called straggling, giving rise to variations in the range of the particles. Straggling is due to the combined effects of different scattering angles and different amounts of energy being lost in each collision, and depends on parameters such as particle momentum and charge, as well as the properties of the shielding material. In addition, slowing down is a stochastic process, which means that the number of interactions required to stop two identical particles in the same medium will vary.

Subiel et al. (2017) investigated this phenomenon of pulse modification by means of Monte Carlo simulations of a 150 MeV electron pulse with an initial pulse length 1 fs, propagating in air and water. The temporal evolution of the particle pulse duration was simulated along the path of propagation in 100 cm air and depths of 1, 10, 20 and 30 cm in water, resulting in pulse lengths of 1.1 fs, 5.0 fs, 100 fs, 0.25 ps and 1 ps, respectively. The pulse was therefore a thousand times longer after passing through 100 cm of air and 30 cm of water, which clearly demonstrates the impact of shielding material on levels of radiation.

The composition of the radiation field determines which dosimetric instrument is suited for a specific workplace. Instruments such as ionization chambers, particle counting devices and solid state detectors are usually employed to monitor complex radiation fields at accelerator facilities. The influence of the pulsed structure of the radiation field on the instrument response differs for these three types of detectors.

5.1 Ionization chambers

An ionization chamber measures the dose delivered at a given point in a radiation field by determining the total amount of charge produced in a cavity filled with a gas. A correction factor has to be applied to the signal output, the so-called *ion recombination correction factor*, due to incomplete charge collection when ion pairs recombine and become charge neutral before being collected at the electrodes. The reliability of dose measurements decreases with increasing recombination of the electron–ion pairs. In radiation fields with a pulsed structure, recombination is often significant.

Standard laboratories, such as the Institute of Physics and Engineering in Medicine and the International Atomic Energy Agency have published codes of practice that define correction factors for small ion chambers used for dosimetry of pulsed clinical radiotherapy beams. However, it has not been confirmed whether such protocols can be used for dosimetry in the case of ultra-short, high-intensity particle beams, rather the opposite. It has been reported that an IBA CC04 ionization chamber exhibited significant ion recombination when employed for primary beam measurements of

165 MeV electrons with a pulse duration of femto- or picoseconds, which could not be corrected for by applying conventional correction factors (Subiel et al., 2017).

The ionization chambers used for radiation protection dosimetry at workplaces have a volume of typically several hundred cm^3 and are thus substantially larger than those used for direct dosimetry of primary beams. The ion-collection time can thus be considered long compared to the period between two pulses, and the chamber will behave as if it were monitoring a continuous radiation field. The correction that should be applied in this case will be different as volume recombination can be neglected, but not initial recombination.

5.2 Solid-state dosimeters

Solid-state dosimeters rely on structural damage or electron and hole trapping induced in a material by irradiation, which can change the properties of materials. All detectors that employ solids as the active detection medium are collectively called solid-state detectors, and include well-known examples such as thermoluminescent, optically stimulated luminescence (OSL) and film dosimeters. Solid-state dosimeters are considered to be reliable in pulsed, high-intensity radiation fields, apart from semiconductors, which can be affected by electromagnetic fields (ICRU 1982, NCRP 2003; Bilski et al., 2006).

5.3 Particle counting devices

Any active detector that detects particle events will, in general, be overwhelmed by the pulses encountered in a high-intensity accelerator environment. Particle counters can be of use in accelerator environments when assessing residual activity or detecting the presence of a radiation field, but they are not suitable for dosimetric purposes (ICRU 1982). Devices that have long dead times, such as proportional and Geiger-Müller counters, are likely to become saturated in high-intensity pulsed fields unless the counting rate in the instrument is significantly below the accelerator pulse rate. Scintillation counters may become nonlinear at higher dose rates due to the inability of photomultipliers to process prompt, high currents.

5.4 Radiation monitoring at the CLF, Rutherford Appleton Laboratory

The Central Laser Facility (CLF) is a leading research facility at the Rutherford Appleton Laboratory, where laser-plasma acceleration is used in a range of research fields. The facility houses two laser systems, ASTRA and VULCAN, which can produce pulses up to the PW regime for the production of high-energy electrons, bremsstrahlung photons, protons, heavy ions and neutrons in ultra-short pulses. Bilski et al. (2006) have described the radiation protection program at the facility, including the instruments employed for monitoring.

The primary radiation fields from the laser systems are bremsstrahlung photons and electrons with an energy spectrum extending up to a few hundred MeV. Doses per shot have been reported to be on the order of 10–100 mSv one meter from the target,

with an average energy < 1 MeV. Protons can be produced with energy spectra extending to about 50 MeV and 1013 particles per shot, with an average energy of about 5 MeV.

Radiation monitoring at CLF follows the principle of defense in depth, meaning that there are several levels of protection, including successive barriers, extending from the initial source to the exterior of the facility building. Both active and passive dosimetric systems are used, and personnel are monitored monthly. Scintillation detectors are used for active monitoring for the control of activated material (Clarke et al., 2014). Environmental radiation monitors consisting of CR-39®[6], OSL detectors and TLDs positioned inside target halls, in selected offices and on the exterior of shielding, are analyzed monthly.

[6] CR-39 is a solid-state nuclear track detector. The designation stands for "Columbia Resin, Batch No. 39" which is a material developed for spectacle lenses. When energetic particles collide with the CR-39 polymer structure, a trail of broken chemical bonds appears.

6 Conclusions

It is well-documented that ultra-high intensity lasers can generate a significant amount of ionizing radiation, and thus radiological safety must be ensured. Appropriate shielding should be used to ensure personnel safety and to comply with legal dose limits and regulations on radiation safety. Radiological characterization studies have been carried out using both experimental measurements and analytical methods, e.g., Monte Carlo simulations.

The radiation fields generated scales with laser intensity, laser energy and the nature of target. A GW class laser system operating in an intensity range of 10^{16} W cm^{-2} can deliver radiation levels that require safety measures, although a very small amount of ionizing radiation is produced per shot. The GW system at CLPU in Salamanca, Spain, has been found to produce dose rates of 0.5 mSv h^{-1} (8 µSv s^{-1}) due to the high repetition rate (kHz), which have been taken into account in radiation safety personnel procedures.

When the laser power is increased above 10 TW, a dose in the order of 1 mSv per shot can be obtained close to the primary electron beam in laser–gas interactions, under certain conditions (Olsovcova et al., 2014a). Apart from electrons, photons constitute a significant contribution to the radiation field. Neutrons are also produced, but their fluence is many orders of magnitude lower than those of electrons and photons. The authors concluded that the yearly dose in the laser control room could reach 0.5 mSv, and that personnel occupancy should be kept to a minimum here. As long as access to certain areas was restricted during experiments, the radiation safety was deemed adequate.

For solid target interactions at a 100 TW laser facility, high dose equivalents were found. It was shown by Borne et al. (2002) that γ-radiation dominated the radiation field, with a 1% contribution from neutrons. As experiments are performed under different conditions, the authors presented results for different combinations of targets and laser energies. These results were extrapolated over a year to obtain a representative value for comparison with international exposure limits. They found that near the interaction chamber, yearly γ doses could exceed 370 mSv. For neutrons, the yearly dose was estimated to be 2 mSv. The authors confirmed the requirement of prohibited access to the experimental area during experiments. The limit for the public of 1 mSv per year, specified in the ICRP 60 recommendations, was not generally exceeded in the working areas surrounding the laser system. In areas where this limit was exceeded, additional measures were suggested to avoid having to classify personnel as radiological workers.

A completely different radiological environment will be encountered at the next generation of laser facilities in the PW power class. At these ultra-high-intensity facilities, the radiation fields will be more similar to those at high-energy accelerators, and radiological safety measures will have to be of a similar standard. Popovici et al. (2017) analytically evaluated the bulk shielding of a 10 PW laser system in the ELI European project. A specific area was assessed, where electron and proton acceleration is planned for high-field quantum electrodynamics experiments, and where the highest energy radiation fields are expected.

At electron acceleration facilities, the radiation field was mainly composed of bremsstrahlung with energies up to tens of GeV. Dose rates in front of a beam dump were found to be a remarkable 100 Sv h^{-1}, but decreased to 10 µSv h^{-1} after the beam dump. Muons and neutrons generated from photon interactions were identified as the

most difficult to shield against. Special muon shielding was proposed after the beam dump. Another topic discussed was that electron acceleration could generate radiation that was differently spatially distributed depending on the beam, e.g., pencil or isotropic beam.

Proton acceleration gives rise to electromagnetic cascading in surrounding material, which results in photons and secondary particles such as neutrons, protons, pions and kaons. In contrast to the case of electron acceleration, the design dose rate constraints were exceeded at some locations. This was due to a higher primary particle flux which generated a higher neutron field. Different measures were suggested to solve this problem, e.g., reducing the laser shot repetition rate or to install supplementary neutron shielding.

As demonstrated in these studies, significant radiation fields can be generated by laser–target interactions. It is therefore important that radiological safety and risks are assessed, and facilities are designed to take this into account. At the highest-intensity facilities, radiation safety measures will be similar to those at conventional high-energy accelerators. However, as the primary source term is localized to the small area around the interaction with the target, which is on the order of μm, this facilitates the control and shielding of radiation hazards.

References

Allison, J., Amako, K., Apostolakis, J., Arce, P., Asai, M., Aso, T., Bagli, E., Bagulya, A., Banerjee, S., Barrand, G., Beck, B., Bogdanov, A., Brandt, D., Brown, J., Burkhardt, H., Canal, P., Cano-Ott, D., Chauvie, S., Cho, K., Cirrone, G., Cooperman, G., Cortés-Giraldo, M., Cosmo, G., Cuttone, G., Depaola, G., et al. (2016). Recent developments in Geant4. Nuclear Instruments and Methods in Physics Research Section A: Accelerators, Spectrometers, Detectors and Associated Equipment, 835, 186 – 225.

Allott, R., Wright, P., Danson, C., Edwards, C., Neely, D., Norreys, P., Rodkiss, D. and Wyborn, B. (2000). Vulcan Petawatt Upgrade: The Radiological Perspective. Annual Report 1999/2000, 177–179. Central Laser Facility, STFC Rutherford Appleton Laboratory, Harwell Oxford, Oxfordshire, United Kingdom.

Amiranoff, F., (2001). Fast electron production in ultra-short high-intensity laser-plasma interaction and its consequences. Meas. Sci. Technol., 12,1795–1800.

Bauer, J., Liang, T., Liu, J., and Rokni, S. (2017). Ionizing Radiation from Terawatt Lasers at SLAC. SLAC National Accelerator Laboratory, Report SLAC-PUB-16458, United States.

Battistoni G., Bauer J., Boehlen T.T., et al. (2016). The FLUKA Code: An Accurate Simulation Tool for Particle Therapy. Frontiers in Oncology 6, 116.

Battistoni, G. Cerutti, F., Fasso, A., Ferrari, A., Muraro, S., Ranft, J., Roesle, S. and Sala, P.R. (2007). The FLUKA code: description and benchmarking, AIP Conference Proceedings 896, 31.

Bechet, S., Versaci, R., Rollet, S., Olsovcova, V., Fajstavr, A., Zakova, M. and Margaronea, D. (2016). Radiation protection of a proton beamline at ELI-Beamlines. J. Instrum., 11, 1–5.

Beg, F.N., Bell, A.R., Dangor, A.E., Danson, C.N., Fews, A.P., Glinsky, M.E., Hammel, B.A., Lee, P., Norreys, P.A., Tatarakis, M. (1997). A study of picosecond laser–solid interactions up to 10^{19} Wcm^{-2}. Phys. Plasmas, 4, 447–457.

Bilski, P., Blomgren, J., d'Errico, F., Esposito, A., Fehrenbacher, G., Fernàndez, Fuchs, F. A., Golnik, N., Lacoste, V., Leuschner, A., Sandri, S., Silari, M., Spurny, F., Wiegel, B. and Wright P. (2006). Complex workplace radiation fields at European high-energy accelerators and thermonuclear fusion facilities. Silari, M. (Ed.), Yellow Report CERN-2006-007.

Borghesi, M., Fuchs, J., Bulanov, S.V., MacKinnon, A.J., Patel P.K. and Roth. M. (2006). Fast ion generation by high-intensity laser irradiation of solid targets and applications. Fusion Sci. Technol., 49, 412–439.

Borne, F., Delacroix, D., Gelé, J.M., Massé, D. and Amiranoff, F. (2002). Radiation protection for an ultra-high intensity laser. Radiat. Prot. Dosimetry, 102, 1, 61–70.

Burza, M., Gonoskov, A., Svensson, K., Wojda, F., Persson, A., Hansson, M., Genoud, G., Marklund, M., Wahlstrom, C.-G. and Lundh, O. (2013). Laser wakefield acceleration using wire produced double density ramps. Phys. Rev. STAB., 16, 011301.

Ceccotti, T., Lévy, T., Réau, F., Popescu, H., Monot, P., Lefebvre, E., Martin, Ph. (2008). Plasma Phys. Control. Fusion, 50, 124006.

Cernaianu, M.O., De Boisdeffre, B., Ursescu, D., Negoita, F., Ur, C.A., Tesileanu, O., Balabanski, D., Ivanoaica, T., Ciubancan, M., Toma, M., Dancus, I. and Gales, S. (2016). Monitoring and control systems for experiments at ELI-NP. Romanian Reports in Physics, Vol. 68, suppl.1, S349–443.

Chao, A.W., Mess, K.H., Tigner, M. and Zimmermann, F. (2013). Handbook of Accelerator Physics and Engineering, Second Edition. Singapore: World Scientific Publishing.

Clarke, R.J., Dorkings, S., Heathcote, R, Markey, K. and Neely, D. (2014). Proton activation history on the Vulcan high-intensity petawatt laser facility. Laser Part. Beams, 32, 455–460.

Clark, E.L., Krushelnick, K., Davies, J.R., Zepf, M., Tatarakis, M., Beg, F.N., Machacek, A., Norreys, P.A., Santala, M.I.K., Watts, I. and Dangor A.E. (2000). Measurements of energetic proton transport through magnetized plasma from intense laser interactions with solids. Phys. Rev. Lett., 84, 670–673.

Clarke, R.J., Neely, D., Edwards, R.D., Wright, P.N.M., Ledingham, K.W.D., Heathcote, R., McKenna, P., Danson, C.N., Brummitt, P.A., Collier, J.L., Hatton, P.E., Hawkes, S. J., Hernandez-Gomez, C., Holligan, P., Hutchinson, M.H.R., Kidd, A.K., Lester, W. J., Neville, D.R., Norreys, P.A., Pepler, D.A., Winstone, T.B., Wyatt, R.W.W. and Wyborn, B. E. (2006). Radiological characterisation of photon radiation from ultra-high-intensity laser-plasma and nuclear interactions. J. Radiol. Prot., 26, 277–286.

Clayton, C.E., Joshi, C., Darrow, C. and Umstadter, D. (1985). Relativistic plasma-wave excitation by collinear optical mixing. Phys. Rev. Lett. 54, 2343–2346.

Corde, S., Ta Phuoc, K., Lambert, G., Fitour, R., Malka, V., Rousse, A., Beck, A. and Lefebvre, E. (2013). Femtosecond x rays from laser-plasma accelerators. Rev. Mod. Phys., 85, 1–48.

Daido, H., Nishiuchi, M. and Pirozhkov, A.S. (2012). Review of laser-driven ion sources and their applications. Rep. Prog. Phys., 75, 1–71.

Desforges, F.G., Paradkar, B.S., Hansson, M., Ju, J., Senje, L., Audet, T.L., Persson, A., Dobosz-Dufrenoy, S., Lundh, O., Maynard, G., Monot, P., Vay, J. L., Wahlstrom, C.-G. and Cros, B. (2014). Dynamics of ionization-induced electron injection in the high density regime of laser wakefield acceleration. Phys. Plasmas, 21, 120703.

Ekerfelt, H. (2015), Parametric study of density down-ramp injection in laser wakefield acceleration, MSc Thesis, Lund Reports on Atomic Physics, Department of Physics, Lund University, Sweden.

Esposito, A. (2011). Radiation protection issues for laser-based accelerators. Radiat. Prot. Dosimetry, 146, 4, 403–406.

Esarey, E., Schroeder, C.B. and Leemans, P. (2009). Physics of laser-driven plasma-based electron accelerators. Rev. Mod. Phys., 81, 1229-1285.

Fasso A. and Rokni, S. (2009). Operational radiation protection in high-energy physics accelerators: Implementation of ALARA in design and operation of accelerators. Radiat. Prot. Dosimetry, 137, 1–2, 94–99.

Ferrari, A., Amato, E., Margarone, D., Cowan, T. and Korn, G. (2013a). Radiation field characterization and shielding studies for the ELI Beamlines facility. Appl. Surf. Sci., 272, 138–144.

Ferrari, A., Amato, E. and Margarone, D. (2013b). Radiation field characterization and shielding studies. AIP Conf. Proc., 1546, 57–62.

Florescu, G.M. and Duliu, O.G. (2016). Shielding activation of petawatt laser facilities in Romania: a FLUKA preliminary evaluation. Radiat. Prot. Dosimetry, 168, 4, 566–569.

Florescu, M.G., Duliu, O.G., Pantazi, D., Ticos, C.M., Sporea, D., Vasilache, R., Ionescu, V. and Oane, M. (2017). Radiological safety assessment for the experimental area of a hyper-intense laser with peak—power of 1PW—CETAL. Radiat. Prot. Dosimetry, 175, 1, 104–109.

Fonseca, C., Mendez, C., Ruiz, C., Fernandez, F. and Roso, L. (2010a). High electron doses from a GW laser interacting with solid aluminum targets. AIP Conf. Proc., 1209, 31–34.

Fonseca, C., Mendez, C., Ruiz, C., Fernandez, F. and Roso, L. (2010b). Measurement of radiation produced by ultra-short laser pulses interacting with solid targets. AIP Conf. Proc., 1231, 223–224.

Hayashi, Y., Fukumi, A., Matsukado, K., Mori, M., Kotaki, H., Kando, M., Chen, L.M., Daito, I., Kondo, S., Kanazawa, S., Yamazaki, A., Ogura, K., Nishiuchi, M., Kado, M., Sagisaka, A., Nakamura, S., Li, Z., Orimo, S., Homma, T. and Daido, H. (2006). Estimation of photon dose generated by a short pulse high power laser. Radiat. Prot. Dosimetry, 121(2), 99–107.

Hooker, S.M. (2013). Developments in laser-driven plasma accelerators. Nature Photon. 7(10), 775–782.

Haines, M.G., Wei, M.S., Beg, F.N. and Stephens, R.B. (2009). Hot-electron temperature and laser-light absorption in fast ignition. Phys. Rev. Lett. 102, 045008.

Hansson, M., Senje, L., Persson, A., Desforges, F.G., Ju, J., Audet, T.L., Dobosz-Dufrénoy, S., Monot, P., Lundh, O., Cros, B. and Wahlström, C.-G. (2014). Enhanced stability of laser wakefield acceleration using dielectric capillary tubes. Phys. Rev. STAB., 17, 031303.

Hansson, M., Aurand, B., Davoine, X., Ekerfelt, H., Svensson, K., Persson, A., Wahlstrom, C.-G. and Lundh, O. (2015). Down-ramp injection and independently controlled acceleration of electrons in a tailored laser wakefield accelerator. Phys. Rev. STAB., 18, 071303.

Hansson, M., Audet, T.L., Ekerfelt, H., Aurand, B., Gallardo Gonzalez, I., Desforges, F.G., Davoine, X., Maitrallain, A., Reymond, S., Monot, P., Persson, A., Dobosz Dufrenoy, S., Wahlstrom, C.-G., Cros, B. and Lundh, O. (2016a). Localization of ionization-induced trapping in a laser wakefield accelerator using a density down-ramp. Plasma Phys. Controlled Fusion, 58, 055009.

Hansson, M., Aurand, B., Ekerfelt, H., Persson, A. and Lundh, O. (2016b). Injection of electrons by colliding laser pulses in a laser wakefield accelerator. Nucl. Instrum. Methods Phys. Res. A, 829, 99–103.

ICRP, (1996). Conversion Coefficients for use in Radiological Protection against External Radiation. ICRP Publication 74. Ann. ICRP 26 (3-4).

ICRP (2010). Conversion coefficients for radiological protection quantities for external radiation exposures. International Commission on Radiological Protection (ICRP) Publication 116, Ann. ICRP 40(2–5).

ICRU (1982). ICRU Report 34: The dosimetry of pulsed radiation. Bethesda, MD: International Commission on Radiation Units and Measurements (ICRU).

Iwase, H., Niita, K. and Nakamura, T., (2002). Development of General-Purpose Particle and Heavy Ion Transport Monte Carlo Code Journal of Nuclear Science and Technology, Taylor & Francis, 39, 1142-1151.

John S. H., H. Grady H., Gregg W. M., Richard E. P. and John T. G., MCNP/X Merger. Avalible from: https://mcnp.lanl.gov/pdf_files/la-ur-08-0533.pdf [Accessed November 30, 2017].

Jones, C., Brenner, C., Stitt, C., Armstrong, C., Rusby, D., Mirfayzi, S., Wilson, L., Alejo, A., Ahmed, H., Allott, R., Butler, N., Clarke, R., Haddock, D., Hernandez-Gomez, C., Higginson, A., Murphy, C., Notley, M., Paraskevoulakos, C., Jowsey, J., McKenna, P., Neely, D., Kar, S., and Scott, T. (2016). Evaluating laser-driven Bremsstrahlung radiation sources for imaging and analysis of nuclear waste packages. J. Hazard. Mater., 318, 694–701.

Leemans, W. P. and Esarey, E. (2009). Laser-driven plasma-wave electron accelerators. Phys. Today, 62, 44–49.

Lefebvre, E., Cochet, N., Fritzler, S., Malka, V., Aléonard, M.-M., Chemin, J.-F., Darbon, S., Disdier, L., Faure, J., Fedotoff, A., Landoas, O., Malka, G., Méot, V., Morel, P., Rabec LeGloahec, M., Rouyer, A., Rubbelynck, Ch., Tikhonchuk, V., Wrobel, R., Audebert, P. and Rousseaux, C. (2003). Electron and photon production from relativistic laser plasma interactions. Nucl. Fusion, 43, 7, 629–633.

Liang, T.T. (2017). Characterization of Ionizing Radiation Generated from Interaction of High-Intensity Laser with Matter. (Doctoral dissertation). Atlanta, USA: Georgia Institute of Technology.

Liang, T., Bauer, J., Cimeno, M., Ferrari, A., Galtier, E., Granados, E., Liu, J., Nagler, B., Prinz, A., Rokni, S., Tran, H. and Woods, M. (2015). Measurements of High-Intensity Laser Induced Ionising Radiation at SLAC. Shielding Aspects of Accelerators, Targets and Irradiation Facilities SATIF-12 Workshop Proceedings, 40–53.

Liang, T., Bauer, J., Cimeno, M., Ferrari, A., Galtier, E., Granados, E., Lee, H.J., Liu, J., Nagler, B., Prinz, A., Rokni, S. and Woods, H.T.M. (2016). Radiation Dose Measurements for high-intensity laser interactions with solid targets at SLAC. Radiat. Prot. Dosimetry, 172, 4, 346–355.

Liang, T., Bauer, J.M., Liu, J.C. and Rokni, S.H. (2017). Bremsstrahlung dose yield for high-intensity short-pulse laser-solid experiments. Radiat. Prot. Dosimetry, 175(3), 304–312.

Lundh, O. (2008). Laser-driven beams of fast ions, relativistic electrons and coherent X-ray photons. (Doctoral dissertation). Lund, Sweden: Department of Physics, Lund University.

Lundh, O. and Rechatin, C. and Faure, J. and Ben-Ismaïl, A. and Lim, J. and De Wagter, C. and De Neve, W. and Malka, V. (2017), Comparison of measured with calculated dose distribution from a 120-MeV electron beam from a laser-plasma accelerator, Medical Physics, 39, 3501-3508.

Macchi, A., Borghesi, M., and Passoni, M. (2013). Ion acceleration by superintense laser-plasma interaction. Rev. Mod. Phys., 85(2), 751–793.

Malka, V., Faure, J., Gauduel, Y., Lefebvre, E., Rousse, A. and Phuoc, K. (2008). Principles and applications of compact laser–plasma accelerators. Nature Phys., 4, 447–453.

Mangles, S.P.D., Thomas, A.G.R., Kaluza, M.C., Lundh, O., Lindau, F., Persson, A., Tsung, F.S., Najmudin, Z., Mori, W.B., Wahlstrom, C.G. and K. Krushelnick (2006). Laser-wakefield acceleration of monoenergetic electron beams in the first plasma-wave period. Phys. Rev. Lett., 96, 215001.

Mitu, I. O., Ivan, C., Negoita, F., Aranghel, D., Bercea, S., Iliescu, E., Petcu, C., Gugiu, M., Popovici, M. A., Ur, C. A., Gales, S. and Zamfiri, N. V. (2016). Radiation protection and safety at ELI-NP. Rom. Rep. Phys., 68, Supplement, S885–S945.

NCRP, (2003). NCRP Report 144: Protection for particle accelerator facilities. Bethesda, Maryland: National Council on Radiation Protection and Measurements (NCRP).

Olsovcova, V., Haley, R., MacFarlene, L., Rus, B. and Griffiths, M. (2014a). Bulk shielding for laser research centre ELI Beamlines. Prog. Nucl. Sci. Technol., 4, 247–251.

Olsovcova, V., Klir, D., Krasa, J., Krus, M., Velyhan, A., Zelenka, Z. and Rus, B. (2014b). Response of dosimeters in the radiation field generated by a TW-class laser system. Radiat. Prot. Dosimetry, 161(1–4), 343–346.

Olsovcova, V., Krus, M., Zelenka, Z., Velyhan, A., Kozlová, M. and Rus, B. (2014c). Radiation protection aspects in the vicinity of TW class laser systems. Prog. Nucl. Sci. Technol., 4, 173–177.

Pelliccioni, M. (1998). Fluence to Dose Equivalent Conversion Data and Radiation Weighting Factors for High Energy Radiation, Radiation Protection Dosimetry 77, 3, 159-170.

Perry, M.D., Sefcik, J.A., Cowan, T., Hatchett, S., Hunt, A., Moran, M., Pennington, D., Snavely, R. and Wilks, S.C. (1999). Hard X-Ray production from high intensity laser solid interactions. Rev. Sci. Instrum., 70(1), 265–269.

Popovici, M. A., Ionica, R. and Cata-Danil, Gh. (2015). Preliminary dosimetric evaluation of electron source terms at PW laser systems. U.P.B. Sci. Bull., Series A, 77(1), 249–263.

Popovici, M. A., Mitu, I. O., Cata-Danil, Gh., Negoita, F. and Ivan, C. (2017). Shielding assessment of high field (QED) experiments at the ELI-NP 10PW laser system. J. Radiol. Prot., 37, 176–188.

Qiu, R., Liu, J.C. Prinz, A.A., Rokni, S.H., Woods M. and Xia Z. (2011). Analysis and mitigation of X-ray hazard generated from high intensity laser–target interactions. SLAC National Accelerator Laboratory, Report SLAC-PUB-14351, United States.

Roth, M. and Schollmeier, M., Ion Acceleration – Target Normal Sheath Acceleration, "Laser-Plasma Interactions and Applications", Scottish Graduate Series (Springer International Publishing, 2013)

Senje, L. (2017). Detector development, source characterization and novel applications of laser ion acceleration, PhD Thesis, Division of Atomic Physics, Department of Physics, Faculty of Engineering, LTH, Lund University.

Stoyer, M.A., Sangster, T.C., Henry, E.A., Cable, M.D., Cowan, T.E., Hatchett, S.P., Key, M.H., Moran, M.J., Pennington, D.M., Perry, M.D., Phillips, T.W., Singh, M.S., Snavely, R.A., Tabak, M. and Wilks S.C. (2001). Nuclear Diagnostic for Petawatt Experiments. Rev. Sci. Instrum., 72(1), 767–772.

Strand Berg, J. (2016). Monte Carlo simulations and measurements of the radiation environment at a laser-plasma accelerator. MSc Thesis, Lund Reports on Atomic Physics, LRAP-529, Department of Physics, Lund University, Sweden.

Strickland, D. and Mourou, G. (1985). Compression of amplified chirped optical pulses. Opt. Commun., 56(3), 219–221.

Svendsen, K. (2017), In-line Phase-Contrast Tomography using Betatron X-rays Produced by a Laser-Plasma Accelerator, MSc Thesis, Lund Reports on Atomic Physics, Department of Physics, Lund University, Sweden.

Svensson, K., Hansson, M., Wojda, F., Senje, L., Burza, M., Aurand, B., Genoud, G., Persson, A., Wahlström, C.-G. and Lundh O. (2016). Supersonic jets of hydrogen and helium for laser wakefield acceleration. Phys. Rev. Accel. Beams, 19(5), 051301.

Subiel, A., Moskvin, V., Welsh, G.H., Cipiccia, S., Reboredo, D., DesRosiers, C., and Jaroszynski, D.A. (2017). Original paper: Challenges of dosimetry of ultra-short pulsed very high energy electron beams. Physica Medica. Available from: https://doi.org/10.1016/j.ejmp.2017.04.029 [Accessed July 19, 2017].

Tajima, T. and Dawson, J.M. (1979). Laser Electron Accelerator. Phys. Rev. Lett., 43, 267–270.

Thaury, C., Guillaume, E., Lifschitz, A., Ta Phuoc, K., Hansson, M., Grittani, G., Gautier, J., Goddet, J.P., Tafzi, A., Lundh, O. and Malka, V. (2015). Shock assisted ionization injection in laser-plasma accelerators. Sci. Rep., 5, 16310.

Torrisi, L. (2014). Ion Acceleration and D-D Nuclear Fusion in Laser-Generated Plasma from Advanced Deuterated Polyethylene. Molecules, 19, 17052–17065.

Vassiliev, O.N. (2017). Monte Carlo Methods for Radiation Transport. Springer International Publishing.

Vlachoudis, V. (2009). FLAIR: A powerful but user friendly graphical interface for FLUKA. Online publication April 2009.

Wilks, S.C. and Kruer, L.K. (1997). Absorption of ultrashort, ultra-intense laser light by solids and overdense plasmas. IEEE J. Quantum Electron., 33, 1954–1968.

Wilks, S.C., Langdon, A.B., Cowan, T.E., Roth, M., Singh, M., Hatchett, S., Key, M.H., Pennington, D., MacKinnon, A. and Snavely, R.A. (2001). Energetic proton generation in ultra-intense laser–solid interactions. Phys. Plasmas, 8, 542–549.

World Nuclear Association, (2017). Nuclear Power in the World Today. Retrieved 2017 September 14 from http://www.world-nuclear.org/information-library/current-and-future-generation/nuclear-power-in-the-world-today.aspx

Yang, B., Qiu, R., Jiao, J., Lu, W., Zhang, Z., Zhou, W., Ma, C., Zhang, H. and Li, J. (2017a). Dosimetric evaluation of laser-driven X-ray and neutron sources utilizing XG-III ps laser with peak power of 300 terawatt. Radiat. Prot. Dosimetry. Online publication 13 April 2017. Available from: https://doi.org/10.1093/rpd/ncx045 [Accessed August 18, 2017].

Yang, B., Qiu, R., Li, J., Lu, W., Wuc, Z. and Li, C. (2017b). Photon dose estimation from ultraintense laser–solid interactions and shielding calculation with Monte Carlo simulation. Radiat. Phys. Chem., 131, 13–21.

Yang, B., Qiu, R., Yu, M., Jiao, J., Lu, W., Yan, Y., Zhang, B., Zhang, Z., Zhou, W., Li, J. and Zhang, H. (2017c). Measurements of X-ray doses and spectra produced by picosecond laser-irradiated solid targets. Appl. Radiat. Isot., 123, 41–48.

This report concerns a study which has been conducted for the Swedish Radiation Safety Authority, SSM. The conclusions and viewpoints presented in the report are those of the author/authors and do not necessarily coincide with those of the SSM.

2019:04

The Swedish Radiation Safety Authority has a comprehensive responsibility to ensure that society is safe from the effects of radiation. The Authority works to achieve radiation safety in a number of areas: nuclear power, medical care as well as commercial products and services. The Authority also works to achieve protection from natural radiation and to increase the level of radiation safety internationally.

The Swedish Radiation Safety Authority works proactively and preventively to protect people and the environment from the harmful effects of radiation, now and in the future. The Authority issues regulations and supervises compliance, while also supporting research, providing training and information, and issuing advice. Often, activities involving radiation require licences issued by the Authority. The Swedish Radiation Safety Authority maintains emergency preparedness around the clock with the aim of limiting the aftermath of radiation accidents and the unintentional spreading of radioactive substances. The Authority participates in international co-operation in order to promote radiation safety and finances projects aiming to raise the level of radiation safety in certain Eastern European countries.

The Authority reports to the Ministry of the Environment and has around 300 employees with competencies in the fields of engineering, natural and behavioural sciences, law, economics and communications. We have received quality, environmental and working environment certification.

Strålsäkerhetsmyndigheten
Swedish Radiation Safety Authority

SE-171 16 Stockholm
Solna strandväg 96

Tel: +46 8 799 40 00
Fax: +46 8 799 40 10

E-mail: registrator@ssm.se
Web: stralsakerhetsmyndigheten.se

Ale Tryckteam AB, Bohus, 2018